

# Inelastic Photoproduction of $J/\psi$ Mesons at HERA

H1 Collaboration

## Abstract

An analysis of inelastic photoproduction of  $J/\psi$  mesons is presented using data collected at the  $ep$  collider HERA corresponding to an integrated luminosity of above  $80 \text{ pb}^{-1}$ . Differential and double differential cross sections are measured in a wide kinematic region:  $60 < W_{\gamma p} < 260 \text{ GeV}$ ,  $1 < p_{t,\psi}^2 < 60 \text{ GeV}^2$  and  $0.05 < z < 0.9$ , where  $z$  is the fraction of the energy of the exchanged photon transferred to the  $J/\psi$  meson in the rest frame of the target proton. Cross sections at  $z \lesssim 0.3$  are presented for the first time. Theoretical calculations within the Colour Singlet Model at NLO for direct photon processes are shown to give a good description of the data in the medium  $z$  region ( $0.3 < z < 0.9$ ) up to the highest  $p_{t,\psi}^2$  values. A calculation using a  $k_t$  factorisation approach in LO in the Colour Singlet Model is also able to describe these data. The data in the full  $z$  range are also compared to LO calculations within a non-relativistic QCD framework including colour octet and colour singlet contributions for direct and resolved photons. It seems possible to reconcile data and theory with modest contributions from colour octet processes. The polarisation of the  $J/\psi$  meson is measured as a function of  $z$  and  $p_{t,\psi}$  and is reasonably described by the theoretical predictions.

To be submitted to Eur. Phys. J. C

C. Adloff<sup>33</sup>, V. Andreev<sup>24</sup>, B. Andrieu<sup>27</sup>, T. Anthonis<sup>4</sup>, A. Astvatsatourov<sup>35</sup>, A. Babaev<sup>23</sup>,  
 J. Bähr<sup>35</sup>, P. Baranov<sup>24</sup>, E. Barrelet<sup>28</sup>, W. Bartel<sup>10</sup>, S. Baumgartner<sup>36</sup>, J. Becker<sup>37</sup>,  
 M. Beckingham<sup>21</sup>, A. Beglarian<sup>34</sup>, O. Behnke<sup>13</sup>, C. Beier<sup>14</sup>, A. Belousov<sup>24</sup>, Ch. Berger<sup>1</sup>,  
 T. Berndt<sup>14</sup>, J.C. Bizot<sup>26</sup>, J. Böhme<sup>10</sup>, V. Boudry<sup>27</sup>, W. Braunschweig<sup>1</sup>, V. Brisson<sup>26</sup>,  
 H.-B. Bröker<sup>2</sup>, D.P. Brown<sup>10</sup>, W. Brückner<sup>12</sup>, D. Bruncko<sup>16</sup>, F.W. Büsser<sup>11</sup>, A. Bunyatyan<sup>12,34</sup>,  
 A. Burrage<sup>18</sup>, G. Buschhorn<sup>25</sup>, L. Bystritskaya<sup>23</sup>, A.J. Campbell<sup>10</sup>, S. Caron<sup>1</sup>,  
 F. Cassol-Brunner<sup>22</sup>, D. Clarke<sup>5</sup>, C. Collard<sup>4</sup>, J.G. Contreras<sup>7,41</sup>, Y.R. Coppens<sup>3</sup>,  
 J.A. Coughlan<sup>5</sup>, M.-C. Cousinou<sup>22</sup>, B.E. Cox<sup>21</sup>, G. Cozzika<sup>9</sup>, J. Cvach<sup>29</sup>, J.B. Dainton<sup>18</sup>,  
 W.D. Dau<sup>15</sup>, K. Daum<sup>33,39</sup>, M. Davidsson<sup>20</sup>, B. Delcourt<sup>26</sup>, N. Delerue<sup>22</sup>, R. Demirchyan<sup>34</sup>,  
 A. De Roeck<sup>10,43</sup>, E.A. De Wolf<sup>4</sup>, C. Diaconu<sup>22</sup>, J. Dingfelder<sup>13</sup>, P. Dixon<sup>19</sup>, V. Dodonov<sup>12</sup>,  
 J.D. Dowell<sup>3</sup>, A. Droutskoi<sup>23</sup>, A. Dubak<sup>25</sup>, C. Duprel<sup>2</sup>, G. Eckerlin<sup>10</sup>, D. Eckstein<sup>35</sup>,  
 V. Efremenko<sup>23</sup>, S. Egli<sup>32</sup>, R. Eichler<sup>36</sup>, F. Eisele<sup>13</sup>, E. Eisenhandler<sup>19</sup>, M. Ellerbrock<sup>13</sup>,  
 E. Elsen<sup>10</sup>, M. Erdmann<sup>10,40,e</sup>, W. Erdmann<sup>36</sup>, P.J.W. Faulkner<sup>3</sup>, L. Favart<sup>4</sup>, A. Fedotov<sup>23</sup>,  
 R. Felst<sup>10</sup>, J. Ferencei<sup>10</sup>, S. Ferron<sup>27</sup>, M. Fleischer<sup>10</sup>, P. Fleischmann<sup>10</sup>, Y.H. Fleming<sup>3</sup>,  
 G. Flügge<sup>2</sup>, A. Fomenko<sup>24</sup>, I. Foresti<sup>37</sup>, J. Formánek<sup>30</sup>, G. Franke<sup>10</sup>, G. Frising<sup>1</sup>,  
 E. Gabathuler<sup>18</sup>, K. Gabathuler<sup>32</sup>, J. Garvey<sup>3</sup>, J. Gassner<sup>32</sup>, J. Gayler<sup>10</sup>, R. Gerhards<sup>10</sup>,  
 C. Gerlich<sup>13</sup>, S. Ghazaryan<sup>4,34</sup>, L. Goerlich<sup>6</sup>, N. Gogitidze<sup>24</sup>, C. Grab<sup>36</sup>, V. Grabski<sup>34</sup>,  
 H. Grässler<sup>2</sup>, T. Greenshaw<sup>18</sup>, G. Grindhammer<sup>25</sup>, T. Hadig<sup>13</sup>, D. Haidt<sup>10</sup>, L. Hajduk<sup>6</sup>,  
 J. Haller<sup>13</sup>, W.J. Haynes<sup>5</sup>, B. Heinemann<sup>18</sup>, G. Heinzelmann<sup>11</sup>, R.C.W. Henderson<sup>17</sup>,  
 S. Hengstmann<sup>37</sup>, H. Henschel<sup>35</sup>, R. Heremans<sup>4</sup>, G. Herrera<sup>7,44</sup>, I. Herynek<sup>29</sup>,  
 M. Hildebrandt<sup>37</sup>, M. Hilgers<sup>36</sup>, K.H. Hiller<sup>35</sup>, J. Hladký<sup>29</sup>, P. Höting<sup>2</sup>, D. Hoffmann<sup>22</sup>,  
 R. Horisberger<sup>32</sup>, A. Hovhannisyan<sup>34</sup>, S. Hurling<sup>10</sup>, M. Ibbotson<sup>21</sup>, Ç. İşsever<sup>7</sup>, M. Jacquet<sup>26</sup>,  
 M. Jaffre<sup>26</sup>, L. Janauschek<sup>25</sup>, X. Janssen<sup>4</sup>, V. Jemanov<sup>11</sup>, L. Jönsson<sup>20</sup>, C. Johnson<sup>3</sup>,  
 D.P. Johnson<sup>4</sup>, M.A.S. Jones<sup>18</sup>, H. Jung<sup>20,10</sup>, D. Kant<sup>19</sup>, M. Kapichine<sup>8</sup>, M. Karlsson<sup>20</sup>,  
 O. Karschnick<sup>11</sup>, F. Keil<sup>14</sup>, N. Keller<sup>37</sup>, J. Kennedy<sup>18</sup>, I.R. Kenyon<sup>3</sup>, S. Kermiche<sup>22</sup>,  
 C. Kiesling<sup>25</sup>, P. Kjellberg<sup>20</sup>, M. Klein<sup>35</sup>, C. Kleinwort<sup>10</sup>, T. Kluge<sup>1</sup>, G. Knies<sup>10</sup>, B. Koblitz<sup>25</sup>,  
 S.D. Kolya<sup>21</sup>, V. Korbel<sup>10</sup>, P. Kostka<sup>35</sup>, S.K. Kotelnikov<sup>24</sup>, R. Koutouev<sup>12</sup>, A. Koutov<sup>8</sup>,  
 J. Kroseberg<sup>37</sup>, K. Krüger<sup>10</sup>, T. Kuhr<sup>11</sup>, T. Kurča<sup>16</sup>, D. Lamb<sup>3</sup>, M.P.J. Landon<sup>19</sup>, W. Lange<sup>35</sup>,  
 T. Laštovička<sup>35,30</sup>, P. Laycock<sup>18</sup>, E. Lebailly<sup>26</sup>, A. Lebedev<sup>24</sup>, B. Leißner<sup>1</sup>, R. Lemrani<sup>10</sup>,  
 V. Lendermann<sup>7</sup>, S. Levonian<sup>10</sup>, M. Lindstroem<sup>20</sup>, B. List<sup>36</sup>, E. Lobodzinska<sup>10,6</sup>,  
 B. Lobodzinski<sup>6,10</sup>, A. Loginov<sup>23</sup>, N. Loktionova<sup>24</sup>, V. Lubimov<sup>23</sup>, S. Lüders<sup>36</sup>, D. Lüke<sup>7,10</sup>,  
 L. Lytkin<sup>12</sup>, N. Malden<sup>21</sup>, E. Malinovski<sup>24</sup>, I. Malinovski<sup>24</sup>, S. Mangano<sup>36</sup>, R. Maraček<sup>25</sup>,  
 P. Marage<sup>4</sup>, J. Marks<sup>13</sup>, R. Marshall<sup>21</sup>, H.-U. Martyn<sup>1</sup>, J. Martyniak<sup>6</sup>, S.J. Maxfield<sup>18</sup>,  
 D. Meer<sup>36</sup>, A. Mehta<sup>18</sup>, K. Meier<sup>14</sup>, A.B. Meyer<sup>11</sup>, H. Meyer<sup>33</sup>, J. Meyer<sup>10</sup>, P.-O. Meyer<sup>2</sup>,  
 S. Mikocki<sup>6</sup>, D. Milstead<sup>18</sup>, S. Mohrdieck<sup>11</sup>, M.N. Mondragon<sup>7</sup>, F. Moreau<sup>27</sup>, A. Morozov<sup>8</sup>,  
 J.V. Morris<sup>5</sup>, K. Müller<sup>37</sup>, P. Murín<sup>16,42</sup>, V. Nagovizin<sup>23</sup>, B. Naroska<sup>11</sup>, J. Naumann<sup>7</sup>,  
 Th. Naumann<sup>35</sup>, G. Nellen<sup>25</sup>, P.R. Newman<sup>3</sup>, F. Niebergall<sup>11</sup>, C. Niebuhr<sup>10</sup>, O. Nix<sup>14</sup>,  
 G. Nowak<sup>6</sup>, M. Nozicka<sup>30</sup>, J.E. Olsson<sup>10</sup>, D. Ozerov<sup>23</sup>, V. Panassik<sup>8</sup>, C. Pascaud<sup>26</sup>,  
 G.D. Patel<sup>18</sup>, M. Peez<sup>22</sup>, E. Perez<sup>9</sup>, A. Petrukhin<sup>35</sup>, J.P. Phillips<sup>18</sup>, D. Pitzl<sup>10</sup>, R. Pöschl<sup>26</sup>,  
 I. Potachnikova<sup>12</sup>, B. Povh<sup>12</sup>, G. Rädcl<sup>1</sup>, J. Rauschenberger<sup>11</sup>, P. Reimer<sup>29</sup>, B. Reisert<sup>25</sup>,  
 C. Risler<sup>25</sup>, E. Rizvi<sup>3</sup>, P. Robmann<sup>37</sup>, R. Roosen<sup>4</sup>, A. Rostovtsev<sup>23</sup>, S. Rusakov<sup>24</sup>, K. Rybicki<sup>6</sup>,  
 J. Samson<sup>36</sup>, D.P.C. Sankey<sup>5</sup>, S. Schätzel<sup>13</sup>, J. Scheins<sup>1</sup>, F.-P. Schilling<sup>10</sup>, P. Schleper<sup>10</sup>,  
 D. Schmidt<sup>33</sup>, D. Schmidt<sup>10</sup>, S. Schmidt<sup>25</sup>, S. Schmitt<sup>10</sup>, M. Schneider<sup>22</sup>, L. Schoeffel<sup>9</sup>,  
 A. Schöning<sup>36</sup>, T. Schörner<sup>25</sup>, V. Schröder<sup>10</sup>, H.-C. Schultz-Coulon<sup>7</sup>, C. Schwanenberger<sup>10</sup>,  
 K. Sedlák<sup>29</sup>, F. Sefkow<sup>37</sup>, V. Shekelyan<sup>25</sup>, I. Sheviakov<sup>24</sup>, L.N. Shtarkov<sup>24</sup>, Y. Sirois<sup>27</sup>,  
 T. Sloan<sup>17</sup>, P. Smirnov<sup>24</sup>, Y. Soloviev<sup>24</sup>, D. South<sup>21</sup>, V. Spaskov<sup>8</sup>, A. Specka<sup>27</sup>, H. Spitzer<sup>11</sup>,

R. Stamen<sup>7</sup>, B. Stella<sup>31</sup>, J. Stiewe<sup>14</sup>, I. Strauch<sup>10</sup>, U. Straumann<sup>37</sup>, M. Swart<sup>14</sup>,  
 S. Tchetchelnitski<sup>23</sup>, G. Thompson<sup>19</sup>, P.D. Thompson<sup>3</sup>, F. Tomasz<sup>14</sup>, D. Traynor<sup>19</sup>, P. Truöl<sup>37</sup>,  
 G. Tsipolitis<sup>10,38</sup>, I. Tsurin<sup>35</sup>, J. Turnau<sup>6</sup>, J.E. Turney<sup>19</sup>, E. Tzamariudaki<sup>25</sup>, S. Udluft<sup>25</sup>,  
 A. Uraev<sup>23</sup>, M. Urban<sup>37</sup>, A. Usik<sup>24</sup>, S. Valkár<sup>30</sup>, A. Valkárová<sup>30</sup>, C. Vallée<sup>22</sup>,  
 P. Van Mechelen<sup>4</sup>, S. Vassiliev<sup>8</sup>, Y. Vazdik<sup>24</sup>, A. Vest<sup>1</sup>, A. Vichnevski<sup>8</sup>, K. Wacker<sup>7</sup>,  
 J. Wagner<sup>10</sup>, R. Wallny<sup>37</sup>, B. Waugh<sup>21</sup>, G. Weber<sup>11</sup>, D. Wegener<sup>7</sup>, C. Werner<sup>13</sup>, N. Werner<sup>37</sup>,  
 M. Wessels<sup>1</sup>, G. White<sup>17</sup>, S. Wiesand<sup>33</sup>, T. Wilksen<sup>10</sup>, M. Winde<sup>35</sup>, G.-G. Winter<sup>10</sup>,  
 Ch. Wissing<sup>7</sup>, M. Wobisch<sup>10</sup>, E.-E. Woehrling<sup>3</sup>, E. Wunsch<sup>10</sup>, A.C. Wyatt<sup>21</sup>, J. Žáček<sup>30</sup>,  
 J. Zálešák<sup>30</sup>, Z. Zhang<sup>26</sup>, A. Zhokin<sup>23</sup>, F. Zomer<sup>26</sup>, and M. zur Nedden<sup>10</sup>

<sup>1</sup> *I. Physikalisches Institut der RWTH, Aachen, Germany<sup>a</sup>*

<sup>2</sup> *III. Physikalisches Institut der RWTH, Aachen, Germany<sup>a</sup>*

<sup>3</sup> *School of Physics and Space Research, University of Birmingham, Birmingham, UK<sup>b</sup>*

<sup>4</sup> *Inter-University Institute for High Energies ULB-VUB, Brussels; Universiteit Antwerpen (UIA), Antwerpen; Belgium<sup>c</sup>*

<sup>5</sup> *Rutherford Appleton Laboratory, Chilton, Didcot, UK<sup>b</sup>*

<sup>6</sup> *Institute for Nuclear Physics, Cracow, Poland<sup>d</sup>*

<sup>7</sup> *Institut für Physik, Universität Dortmund, Dortmund, Germany<sup>a</sup>*

<sup>8</sup> *Joint Institute for Nuclear Research, Dubna, Russia*

<sup>9</sup> *CEA, DSM/DAPNIA, CE-Saclay, Gif-sur-Yvette, France*

<sup>10</sup> *DESY, Hamburg, Germany*

<sup>11</sup> *Institut für Experimentalphysik, Universität Hamburg, Hamburg, Germany<sup>a</sup>*

<sup>12</sup> *Max-Planck-Institut für Kernphysik, Heidelberg, Germany*

<sup>13</sup> *Physikalisches Institut, Universität Heidelberg, Heidelberg, Germany<sup>a</sup>*

<sup>14</sup> *Kirchhoff-Institut für Physik, Universität Heidelberg, Heidelberg, Germany<sup>a</sup>*

<sup>15</sup> *Institut für experimentelle und Angewandte Physik, Universität Kiel, Kiel, Germany*

<sup>16</sup> *Institute of Experimental Physics, Slovak Academy of Sciences, Košice, Slovak Republic<sup>e,f</sup>*

<sup>17</sup> *School of Physics and Chemistry, University of Lancaster, Lancaster, UK<sup>b</sup>*

<sup>18</sup> *Department of Physics, University of Liverpool, Liverpool, UK<sup>b</sup>*

<sup>19</sup> *Queen Mary and Westfield College, London, UK<sup>b</sup>*

<sup>20</sup> *Physics Department, University of Lund, Lund, Sweden<sup>g</sup>*

<sup>21</sup> *Physics Department, University of Manchester, Manchester, UK<sup>b</sup>*

<sup>22</sup> *CPPM, CNRS/IN2P3 - Univ Mediterranee, Marseille - France*

<sup>23</sup> *Institute for Theoretical and Experimental Physics, Moscow, Russia<sup>l</sup>*

<sup>24</sup> *Lebedev Physical Institute, Moscow, Russia<sup>e</sup>*

<sup>25</sup> *Max-Planck-Institut für Physik, München, Germany*

<sup>26</sup> *LAL, Université de Paris-Sud, IN2P3-CNRS, Orsay, France*

<sup>27</sup> *LPNHE, Ecole Polytechnique, IN2P3-CNRS, Palaiseau, France*

<sup>28</sup> *LPNHE, Universités Paris VI and VII, IN2P3-CNRS, Paris, France*

<sup>29</sup> *Institute of Physics, Academy of Sciences of the Czech Republic, Praha, Czech Republic<sup>e,i</sup>*

<sup>30</sup> *Faculty of Mathematics and Physics, Charles University, Praha, Czech Republic<sup>e,i</sup>*

<sup>31</sup> *Dipartimento di Fisica Università di Roma Tre and INFN Roma 3, Roma, Italy*

<sup>32</sup> *Paul Scherrer Institut, Villigen, Switzerland*

<sup>33</sup> *Fachbereich Physik, Bergische Universität Gesamthochschule Wuppertal, Wuppertal, Germany*

<sup>34</sup> *Yerevan Physics Institute, Yerevan, Armenia*

<sup>35</sup> *DESY, Zeuthen, Germany*

<sup>36</sup> *Institut für Teilchenphysik, ETH, Zürich, Switzerland<sup>j</sup>*

<sup>37</sup> *Physik-Institut der Universität Zürich, Zürich, Switzerland<sup>j</sup>*

<sup>38</sup> *Also at Physics Department, National Technical University, Zografou Campus, GR-15773 Athens, Greece*

<sup>39</sup> *Also at Rechenzentrum, Bergische Universität Gesamthochschule Wuppertal, Germany*

<sup>40</sup> *Also at Institut für Experimentelle Kernphysik, Universität Karlsruhe, Karlsruhe, Germany*

<sup>41</sup> *Also at Dept. Fis. Ap. CINVESTAV, Mérida, Yucatán, México<sup>k</sup>*

<sup>42</sup> *Also at University of P.J. Šafárik, Košice, Slovak Republic*

<sup>43</sup> *Also at CERN, Geneva, Switzerland*

<sup>44</sup> *Also at Dept. Fis. CINVESTAV, México City, México<sup>k</sup>*

<sup>a</sup> *Supported by the Bundesministerium für Bildung und Forschung, FRG, under contract numbers 05 H1 1GUA /1, 05 H1 1PAA /1, 05 H1 1PAB /9, 05 H1 1PEA /6, 05 H1 1VHA /7 and 05 H1 1VHB /5*

<sup>b</sup> *Supported by the UK Particle Physics and Astronomy Research Council, and formerly by the UK Science and Engineering Research Council*

<sup>c</sup> *Supported by FNRS-FWO-Vlaanderen, IISN-IIKW and IWT*

<sup>d</sup> *Partially Supported by the Polish State Committee for Scientific Research, grant no. 2P0310318 and SPUB/DESY/P03/DZ-1/99 and by the German Bundesministerium für Bildung und Forschung*

<sup>e</sup> *Supported by the Deutsche Forschungsgemeinschaft*

<sup>f</sup> *Supported by VEGA SR grant no. 2/1169/2001*

<sup>g</sup> *Supported by the Swedish Natural Science Research Council*

<sup>i</sup> *Supported by the Ministry of Education of the Czech Republic under the projects INGO-LA116/2000 and LN00A006, by GAUK grant no 173/2000*

<sup>j</sup> *Supported by the Swiss National Science Foundation*

<sup>k</sup> *Supported by CONACyT*

<sup>l</sup> *Partially Supported by Russian Foundation for Basic Research, grant no. 00-15-96584*

# 1 Introduction

The production of  $J/\psi$  mesons,  $ep \rightarrow e J/\psi X$ , has been studied intensively at HERA [1–4]. The high available energy allows the contributing mechanisms to be studied in a wide kinematic range in both  $Q^2$  and  $W_{\gamma p}$ . Here  $Q^2$  is the negative squared four-momentum of the exchanged photon and  $W_{\gamma p}$  is the centre of mass energy of the photon proton system. In this paper we concentrate on the inelastic process where, in the proton rest system, the  $J/\psi$  meson carries a fraction  $z \leq 0.9$  of the photon energy in contrast to diffractive processes where this fraction is close to 1. The inelastic process is dominated by boson gluon fusion: a photon emitted from the incoming lepton interacts with a gluon from the proton to produce a  $c\bar{c}$  pair which subsequently forms the  $J/\psi$  meson. Here we will consider only interactions of quasi-real photons<sup>1</sup>,  $Q^2 \simeq 0$ . In this case the photon can either couple to the  $c$  quark directly (“direct” processes, Fig. 1a or b) or can interact via its hadronic component (“resolved” processes, Fig. 1c).

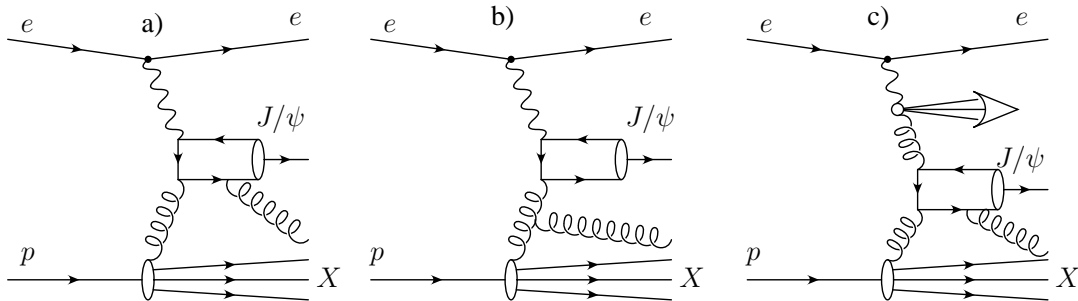


Figure 1: *Generic Feynman diagrams for inelastic  $J/\psi$  production. a,b) direct photon processes; c) resolved photon process. In diagrams a) and c) the  $c\bar{c}$  pair leading to the formation of the  $J/\psi$  can be in a colour singlet or octet state while in b) it can only be in a colour octet state. Additional soft gluons emitted during the hadronisation process are not shown.*

Many models have been suggested to describe inelastic  $J/\psi$  production in the framework of perturbative Quantum Chromodynamics (pQCD) such as the Colour Singlet Model (CSM) [5], the colour evaporation model [6] and soft colour interactions [7]. Recently, discussions have focussed on calculations based on a factorisation theorem in a non-relativistic QCD approach (NRQCD) [8]. These theoretical descriptions differ in many details. One important difference concerns the states they allow for the intermediate  $c\bar{c}$  pair produced in the hard boson gluon interaction in terms of angular momentum and colour. Furthermore they differ in the non-perturbative description of the transition from the intermediate  $c\bar{c}$  pair to the  $J/\psi$  meson.

In the CSM it is assumed that the intermediate  $c\bar{c}$  pair is only produced in the quantum state of the  $J/\psi$  meson, i.e. in a colour singlet state with spin 1 and no orbital angular momentum. However, the CSM predicts prompt production rates of  $J/\psi$  and  $\psi'$  mesons in  $p\bar{p}$  interactions, which are lower by more than an order of magnitude than the rates seen by the CDF collaboration [9]. The NRQCD approach, in which contributions from  $c\bar{c}$  pairs in colour octet states are predicted in addition to colour singlet contributions, can accommodate the measured  $p\bar{p}$  cross sections. Long distance matrix elements (LDMEs) are used to describe the transition of the various intermediate  $c\bar{c}$  states to the  $J/\psi$  meson. In previous publications [2, 3] it was shown

<sup>1</sup>The regime of virtual photons is studied in [1].

that in photoproduction at HERA the colour octet contributions are not observed with the magnitude predicted by leading order NRQCD calculations, in which LDMEs are used which are extracted, also in leading order (LO), from  $p\bar{p}$  data. However the data were well described by the next-to-leading order (NLO) calculations in the CSM. Subsequently theoretical efforts were made to improve the simultaneous description of the photoproduction and  $p\bar{p}$  processes within NRQCD, e.g. the effects of higher order corrections have been estimated in the extraction of the LDMEs as well as in the photoproduction amplitudes [10–13].

Since our first publication [2] the amount of data taken by the H1 experiment has increased and allows more detailed investigations in a larger region of phase space. Here we present an analysis in an extended  $z$  region,  $0.05 < z < 0.9$  covering  $60 < W_{\gamma p} < 260$  GeV and transverse momenta of the  $J/\psi$ ,  $1 \leq p_{t,\psi}^2 \leq 60$  GeV<sup>2</sup>. In the medium  $z$  region, which has been analysed previously, mainly direct photon processes are expected. At the lowest  $z$  values resolved processes are expected to contribute to the cross section in addition.

The data in the medium  $z$  range are compared with two sets of calculations within the CSM, namely a NLO calculation [14] and a LO Monte Carlo computation [15, 16] using a “ $k_t$  factorisation” approach<sup>2</sup> [17, 18]. A comparison of the data with LO calculations in the NRQCD framework including colour octet contributions is carried out over the full range  $0.05 \leq z \leq 0.9$ . The decay angular distribution of the  $J/\psi$  meson is analysed yielding information on the polarisation of the  $J/\psi$  meson and the results are compared with predictions in the NRQCD framework both with and without colour octet contributions [19] and in a  $k_t$  factorisation approach [20].

## 2 Theoretical Models for $J/\psi$ Production

The salient features of the relevant theoretical calculations are briefly summarised here. A comprehensive overview can be found in [21].

In the Colour Singlet Model [5] for direct photon processes the  $J/\psi$  meson is produced via  $\gamma g \rightarrow c\bar{c}[1,^3S_1] + g$ , where the quantum state of the  $c\bar{c}$  pair is described in spectroscopic notation<sup>3</sup>. The transition from the  $c\bar{c}$  pair to the  $J/\psi$  meson is calculated in potential models and can be related to the measured leptonic decay width of the  $J/\psi$  meson. For photoproduction, full NLO calculations, i.e. up to order  $\alpha_s^3$ , where  $\alpha_s$  denotes the strong coupling, are available for the direct process [14]. The NLO contributions lead to an increase of the cross sections by roughly a factor 2, dependent on the transverse momentum of the  $J/\psi$  meson. The resolved photon process is expected to be dominated by  $gg \rightarrow c\bar{c}[1,^3S_1] + g$ , for which only LO calculations are available.

These CSM calculations are performed using standard collinear gluon density distributions. An alternative  $k_t$  factorisation approach [17, 18] has recently been successfully applied to the description of a variety of processes [15]. In this approach the  $J/\psi$  production process is factorised into a  $k_t$  dependent gluon density and a matrix element for off-shell partons. A LO calculation within this approach is implemented in the Monte Carlo generator CASCADE [15].

<sup>2</sup>Here “ $k_t$ ” refers to a transverse momentum component of the gluon entering the hard interaction.

<sup>3</sup>Spectroscopic notation:  $^{2S+1}L_J$  where  $S$ ,  $L$  and  $J$  denote the spin, orbital and total angular momenta of the  $c\bar{c}$  system that is produced in the hard process. The first number in the square bracket indicates the colour state of the  $c\bar{c}$  pair.

In the NRQCD approach the  $J/\psi$  production amplitude factorises into short distance terms for the creation of colour octet or singlet  $c\bar{c}$  states with definite angular momenta and long distance terms describing the transition of these  $c\bar{c}$  states to the  $J/\psi$  meson. A double expansion in the strong coupling parameter  $\alpha_s$  and  $v$ , the relative velocity of quark and antiquark, is obtained. In specific calculations [10, 11, 21] only the most important contributions are kept. In this expansion the lowest order term in  $v$  is the colour singlet term. Assuming that all other terms do not contribute, the CSM is recovered.

Whereas the short distance amplitudes are calculable in pQCD the LDMEs must be determined from experimental data at present. They are assumed to be process independent, i.e. they can be determined for example in  $p\bar{p}$  collisions or from  $B$  decays and can then be used in predictions for photoproduction. Calculations for photoproduction based on the NRQCD approach are available in LO taking into account the contributions  $[1, {}^3S_1]$ ,  $[8, {}^3S_1]$ ,  $[8, {}^1S_0]$  and  $[8, {}^3P_{J=0,1,2}]$ . The relative strength of the colour octet contributions depends crucially on the size of the corresponding LDMEs. Unfortunately the values for the LDMEs important at HERA still show large uncertainties (a summary can be found in [21]). Early extractions of the LDMEs from  $p\bar{p}$  data were performed in LO. Subsequent estimates of higher order effects led to considerably smaller values [10–13].

The first comparisons of NRQCD calculations with photoproduction data [2, 3] revealed large discrepancies between data and theory at high values of  $z$ , the theory being a factor 3-5 higher than the data. In later calculations resumming of soft gluon emissions within the NRQCD expansion [11] was shown to damp the colour octet contributions at high  $z$ . The region of validity of these calculations is restricted to  $J/\psi$  production with high transverse momentum, a region where experimental data suffer from limited statistics.

All theoretical calculations contain a number of free parameters, e.g. the parton density distributions, the values of  $\alpha_s$  and the charm quark mass  $m_c$  as well as the choice of the renormalisation and factorisation scales. In the NRQCD approach the values of the octet LDMEs are additional parameters. The comparison with the data in the NRQCD approach also suffers from the uncertainties associated with LO calculations. Although the NLO terms have not been calculated in the NRQCD approach similar effects as in the CSM may be expected, where the NLO terms lead to an increase of the cross section of typically a factor 2 with a strong  $p_{t,\psi}$  dependence. Measurements of the polarisation of the  $J/\psi$  meson should help to discriminate between different theoretical descriptions, independently of normalisation uncertainties.

Table 1 gives an overview of the calculations available in the low and medium  $z$  regions.

$z$ region	Contributing Process	Available theoretical calculations
medium $z$ ( $0.3 < z < 0.9$ )	direct photon process	CSM NLO and LO, NRQCD LO $k_t$ factorisation
low $z$ ( $0.05 < z < 0.45$ )	direct + resolved photon processes	CSM LO, NRQCD LO

Table 1: *Overview of theoretical calculations compared with the present data in the medium and low  $z$  regions.*

### 3 Experimental Conditions

The data presented here were collected in the years 1996–2000 and correspond to a total integrated luminosity of  $(87.5 \pm 1.3) \text{ pb}^{-1}$ . HERA was operated with electrons or positrons of 27.5 GeV. The proton beam energy was 820 GeV before 1998 and 920 GeV since.

#### 3.1 Detector and Event Selection

The experimental methods are similar to those described in [1, 2, 22]. Details of the detector and the analysis can be found in [23] and [24], respectively.  $J/\psi$  mesons are detected via the decays  $J/\psi \rightarrow \mu^+\mu^-$  (branching fraction of  $(5.88 \pm 0.10)\%$  [26]). Reconstructed tracks in the central tracking detector (CTD) are identified as muons either because they produce minimal ionisation in the main (liquid argon, LAr) calorimeter or because they are linked to a track in the instrumented iron return yoke of the magnet (muon detector). The trigger requirements rely on signals from track chambers and the muon detector, so for consistency at least one muon has to be reconstructed in the muon detector.

The event sample is subdivided into three (partially overlapping) datasets to facilitate specific analyses. The datasets differ in the kinematic requirements for  $z$ ,  $W_{\gamma p}$  and the minimum muon momentum  $p_{\mu}^{\text{min}}$  imposed in the selection (see table 2). Dataset I is a medium  $z$  selection,  $0.3 < z < 0.9$ . Dataset II emphasizes the low  $z$  region and the selection imposes a restriction in the polar angle of the muons to suppress background at  $z \lesssim 0.2$ . The  $z$  range,  $0.05 < z < 0.45$ , is chosen to overlap with dataset I. The  $W_{\gamma p}$  ranges for the datasets I and II are adjusted to give high acceptance in the corresponding  $z$  range. This results in a reduced  $W_{\gamma p}$  range for dataset II. In order to determine the differential cross section  $d\sigma/dz$  in the full  $z$  range, a third sample, dataset III, is defined, which covers the same  $W_{\gamma p}$  region as dataset II but covers a complementary  $z$  range identical to that of dataset I.

In selecting  $J/\psi$  events two identified muons with momenta  $p_{\mu} > 1.1$  GeV are required (datasets I and III) and  $p_{\mu} > 0.8$  GeV for dataset II. One of the muons must be reconstructed in the muon detector and has to have a momentum  $p_{\mu} > 1.8$  GeV. In addition to the decay muons at least three additional tracks are required in order to suppress diffractive  $J/\psi$  contributions. Furthermore a cut on the transverse momentum of the muon pair,  $p_{t,\psi} > 1$  GeV, is applied. The restriction to photoproduction is made by removing events with a cluster of energy above 8 GeV in the electromagnetic part of the calorimeter. The mean  $Q^2$  is then  $0.05 \text{ GeV}^2$ .

The distribution of the invariant mass of the two muon candidates after these cuts is shown for datasets I and II in Fig. 2. There is a considerable non-resonant background in regions of low

Dataset	$z$	$W_{\gamma p}$ [ GeV ]	$\theta_{\mu}$ [°]	$p_{\mu}^{\text{min}}$ [ GeV ]
I	0.3 - 0.9	60 - 240	20 - 160	1.1
II	0.05 - 0.45	120 - 260	20 - 140	0.8
III	0.3 - 0.9	120 - 260	20 - 160	1.1

Table 2: Overview of kinematic ranges and selection criteria for the three datasets. All datasets are restricted to  $Q^2 < 1\text{GeV}^2$  and  $p_{t,\psi} > 1\text{GeV}$ .

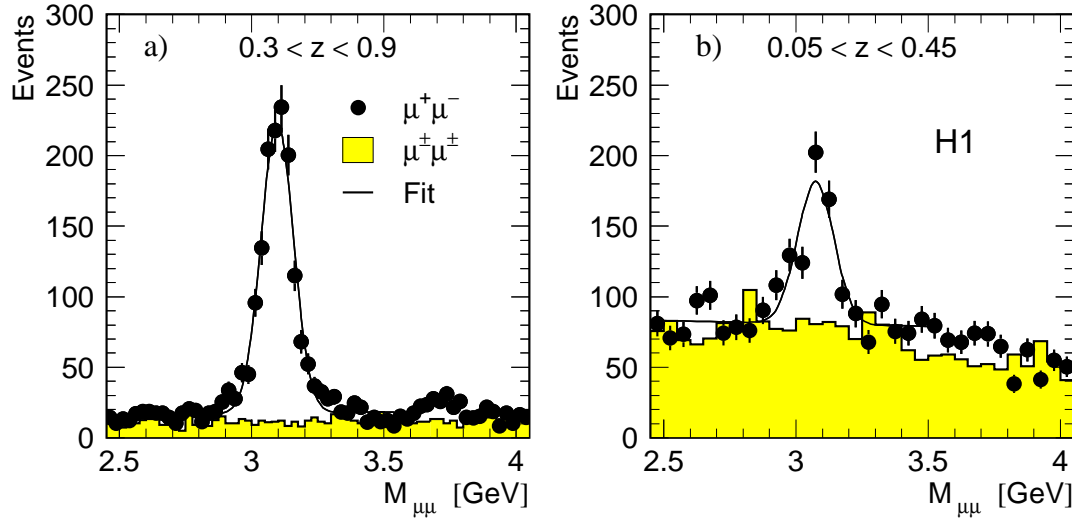


Figure 2: *Distribution of the invariant mass of the muon pairs after all selection cuts a) in the range  $0.3 < z < 0.9$ ,  $60 < W_{\gamma p} < 240$  GeV and  $p_{t,\psi} > 1$  GeV (dataset I) and b) in the range  $0.05 < z < 0.45$ ,  $120 < W_{\gamma p} < 260$  GeV and  $p_{t,\psi} > 1$  GeV (dataset II). The data points with statistical error bars show the unlike sign combinations, the histograms the like sign combinations. The lines are fits as described in the text.*

$z$  due mainly to misidentified leptons as can be seen from the distribution of like sign pairs in Fig. 2b. The following procedure is adopted to extract the number of signal events in a given analysis bin: the mass distribution is fitted in the interval  $2.45 < M_{\mu\mu} < 3.45$  GeV with a superposition of a Gaussian to describe the signal and a function linear in mass to describe the background. The width and position of this Gaussian are determined from an overall fit to the data and are then fixed. The number of signal events is obtained by counting the number of muon pairs in the interval  $2.9 < M_{\mu\mu} < 3.3$  GeV and subtracting the fitted background in this interval. By varying the shape assumed for the background the systematic error in the number of signal events is estimated to be 5-15% at low  $z$  values and less than 1% at higher  $z$  values.

## 3.2 Kinematics

The following kinematic variables are used to describe  $J/\psi$  production: the square of the  $ep$  centre of mass energy,  $s = (k + p)^2$ , the negative squared four-momentum transfer  $Q^2 = -q^2$  and the photon proton center of mass energy  $W_{\gamma p} = \sqrt{(p + q)^2}$ . Here  $k$ ,  $p$  and  $q$  are the four-momenta of the incident lepton, proton and the exchanged photon, respectively. The scaled energy transfer  $y = q \cdot p / k \cdot p$  is the energy fraction transferred from the lepton to the hadronic final state in the proton rest frame. Neglecting the lepton and proton masses, a good approximation is  $W_{\gamma p}^2 \approx ys$  in the limit of  $Q^2 \simeq 0$  considered here. The fraction of the photon energy transferred to  $J/\psi$  meson in the proton rest frame is given by

$$z = \frac{p_\psi \cdot p}{q \cdot p},$$

where  $p_\psi$  denotes the  $J/\psi$  four-momentum.

The kinematic variables are reconstructed using the Jacquet-Blondel method [25]:

$$y = \frac{1}{2E_e} \sum_{had} (E - p_z),$$

$$z = \frac{(E - p_z)_{J/\psi}}{2y E_e},$$

where  $E_e$  denotes the energy of the incoming lepton.  $(E - p_z)_{J/\psi}$  is calculated from the  $J/\psi$  decay muons and  $\sum_{had}$  runs over all final state hadrons including the  $J/\psi$  meson. In the calculation of the final state hadronic energy a combination of tracks reconstructed in the CTD and energy depositions in the LAr and SpaCal calorimeters is used.

The resolution for  $W_{\gamma p}$  and  $p_{t,\psi}^2$  is much smaller than the width of the chosen analysis intervals. The absolute resolution for  $z$  is typically 0.08 for  $z > 0.4$  and 0.02 at  $z \sim 0.1$ . The size of the  $z$  bins is chosen so that in the Monte Carlo simulation the fraction of events reconstructed in the bin in which they were generated is above 60%.

### 3.3 Comparison of Data and Simulation

The Monte Carlo program EPJPSI [27] is used to generate two types of simulated datasets. The first contains  $J/\psi$  events from direct photon gluon fusion, the second from gluon gluon fusion corresponding to the main expected contribution to the resolved photon component. Both processes are calculated in the Colour Singlet Model in LO. Relativistic corrections are included, which enhance the cross section at high  $z$  values [27]. The proton and photon gluon densities in the simulation are taken from MRS(A') [28] and GRV-LO [29], respectively. The QCD renormalisation and factorisation scales are chosen as  $M_{J/\psi}$ . Parton showers are simulated but their effect is small.

The procedure to extract cross sections relies on the detailed simulation of the H1 detector response. Particular care is taken to adjust the efficiency functions for the muon identification and trigger algorithms in order to achieve a reliable description as a function of the muon momenta and angles. This adjustment is performed using high statistics datasets from diffractive  $J/\psi$  production [24]. Remaining differences between data and simulation are taken into account in the systematic error.

The two simulated datasets for direct and resolved photon processes are merged and normalised to the data, as follows (see also Fig. 3a–c and d–f for the medium and low  $z$  datasets I and II, respectively). First, the generated events of the direct photon simulation are reweighted in  $p_{t,\psi}^2$  according to a parametrisation of the measured distribution in the medium  $z$  range. The simulation is then normalised to the data in the range  $0.45 < z < 0.9$ , where backgrounds from diffractive and resolved photon processes are expected to be negligible. Extrapolation of the simulation into the low  $z$  region shows that 35  $J/\psi$  mesons are expected in the interval  $0.05 < z < 0.15$  whereas 80  $J/\psi$  meson candidates are observed. This excess of observed events over the direct photon simulation is attributed to the resolved photon component, which is normalised accordingly. In principle a contribution from  $b\bar{b}$  pairs decaying to  $J/\psi$  mesons should also be taken into account. However, the theoretical and experimental uncertainties are

still large for  $b\bar{b}$  production, and the process is thus neglected here (see also discussion in the next section).

A contribution of resolved photons of about 50% at  $0.05 < z < 0.15$  is obtained falling to 10% for  $0.15 < z < 0.3$  and being negligible for  $z > 0.3$  (Fig. 3e). Note that the resolved component is not reweighted in  $p_{t,\psi}^2$  since good agreement of the superposition of the two simulations with the data is found (Fig. 3f). This may, however, be fortuitous because of the neglected  $b$  contribution, which is expected to be important particularly at high values of  $p_{t,\psi}^2$ . Current simulations (AROMA [30] and EPJPSI [27]) normalised to the measured value for  $ep \rightarrow ebb\bar{X}$  with  $Q^2 < 1 \text{ GeV}^2$  of  $(14.8 \pm 1.3_{-2.8}^{+3.3})\text{nb}$  [31], predict  $b$  contributions of the order of 50% or more in the highest analysis interval  $20 < p_{t,\psi}^2 < 40 \text{ GeV}^2$ .

### 3.4 Other Contributions to $J/\psi$ Production

After the selection cuts described in section 3.1 the  $J/\psi$  sample is dominated by inelastic  $J/\psi$  production, in which the  $J/\psi$  is directly produced from the  $c\bar{c}$  pair in the boson gluon fusion process. However, contributions remain from both the diffractive and inelastic production of  $\psi(2S)$  mesons, the production of  $b$  flavoured hadrons and possibly also from  $\chi_c$  states. The estimated amounts of these feeddown processes are summarised in Table 3. Note that these contributions are *not* subtracted, either because they are negligible, such as diffractive backgrounds, or, because the dependence on the kinematic variables has not been measured and is only poorly known from theory, as in production of  $b\bar{b}$  pairs with subsequent decays to  $J/\psi$  mesons.

Contributions from diffractively produced  $J/\psi$  and  $\psi(2S)$  mesons are effectively suppressed by the requirements of at least three tracks in addition to the decay muons and  $p_{t,\psi}^2 > 1 \text{ GeV}^2$ . The remaining contribution from the cascade decay of  $\psi(2S)$  is estimated with a simulation of diffractive  $\psi(2S)$  production using the DIFFVM generator program [32]. DIFFVM is normalised to the observed signal of  $\psi(2S) \rightarrow J/\psi\pi^+\pi^-$  in a sample of events with exactly four tracks. A residual contribution from diffractive  $\psi(2S)$  production of about 3% in the highest  $z$  bin is inferred. Averaged over the total  $z$  range this background is less than 1% in the medium  $z$  region and negligible at low  $z$ .

Source	Contribution (%)	
	Dataset I, III	Dataset II
Diffractive $\psi(2S) \rightarrow J/\psi + X$ ( $0.75 < z < 0.9$ )	1 (3)	-
Inelastic $\psi(2S) \rightarrow J/\psi + X$	15	15
$b \rightarrow J/\psi + X$ ( $0.3 < z < 0.45$ )	5 (19)	25
$\chi_c \rightarrow J/\psi + \gamma$	1	7

Table 3: *Estimated contributions from other processes to the measured  $J/\psi+X$  data sample in addition to inelastic boson gluon fusion. The amounts in parentheses refer to the  $z$  bins in parentheses.*

The inelastic photoproduction of  $\psi(2S)$  mesons with subsequent decays to  $J/\psi$  mesons is expected to contribute 15% to  $J/\psi$  production [14] and to show similar dependences on the kinematic variables because the production processes are the same.

The contribution from the decay of  $b$  flavoured hadrons can only be estimated with large uncertainties, since few measurements exist [31] and these considerably exceed current theoretical estimates. Using the EPJPSI generator program and normalizing the production cross section to the measured value for  $ep \rightarrow ebb\bar{X}$  with  $Q^2 < 1 \text{ GeV}^2$  [31], a contribution of  $(25 \pm 6)\%$  due to  $b \rightarrow J/\psi + X$  is estimated in the kinematic region of dataset II (see also Fig. 3). At higher  $z$  and lower  $W_{\gamma p}$  the background fraction is smaller. For example in the lowest  $z$  bin of dataset I a contribution of  $(19 \pm 5)\%$  is found which would correspond to  $5 \pm 1\%$  in the total  $z$  region of dataset I.

A further potential contribution comes from  $\chi_c$  decays,  $\chi_c \rightarrow \gamma + J/\psi$ . The Colour Singlet Model predicts that  $\chi_c$  mesons can only be produced in resolved photon processes due to quantum number conservation. From EPJPSI 7% of the total resolved contribution is estimated to arise from this source. The production of  $\chi_c$  mesons is possible also in direct photon gluon fusion via colour octet  $^3S_1$  states, which would result in a contribution of less than 1% in the medium  $z$  region [21].

### 3.5 Systematic Uncertainties

The estimated systematic errors on the cross sections are listed in Table 4. The uncertainty from the track reconstruction is based on an error of 2% for the efficiency per track and takes into account the observed track multiplicity distribution. The systematic error of the total hadronic energy includes the uncertainty of the calorimeter energy scales (4% for the LAr, and 10% for the SpaCal) and leads to cross section error estimates of 4% (6%) in the medium (low)  $z$  regions. The systematic errors in the muon identification and trigger efficiencies are estimated from the residual differences between data and simulation. The error in the determination of the event numbers in the analysis bins is estimated by changing the description of the non-resonant background from a linear dependence on the invariant mass to a power law. The error on the acceptance due to restricting the polar angle of the decay muons is obtained by using different proton and photon parton densities which influence the  $W_{\gamma p}$  distribution. In general the changes in the acceptance are small. A significant uncertainty is found only at large  $W_{\gamma p}$  in dataset I and at small  $W_{\gamma p}$  in dataset II. The uncertainty in the acceptance at low  $z$  due to the modelling of the  $z$  dependence is found to be 4%. The low  $z$  dataset II contains a sizeable contribution from  $b \rightarrow J/\psi + X$ . The effect on the acceptance is estimated using the EPJPSI simulation of  $b\bar{b}$  production with a relative contributions as in table 3. The decay angular distribution of the  $J/\psi$  meson has an influence on the acceptance mainly in the medium  $z$  region. Varying the decay angular distribution of the  $J/\psi$  meson within the measured uncertainties<sup>4</sup> changes the acceptance by  $\pm 8\%$  nearly independently of other variables.

---

<sup>4</sup>The parameter  $\lambda$  in equation (1) in section 4.5 is varied from 0 (used in the simulation) to +1 or -0.5.

Source	Uncertainty [%]	
	Dataset I, III	Dataset II
Track reconstruction efficiency	6	6
Muon identification efficiency	3	7
Calorimeter energy scales	4	6
Signal events	< 1	5 – 15
Trigger efficiency	6	10
Acceptance: PDFs	4 – 8	5 – 10
$z$ dependence	-	4
$J/\psi$ decay ang. distr.	8	7
$b \rightarrow J/\psi + X$	< 1	3 – 12
Integrated luminosity	1.5	
Branching ratio	1.7	
Total	13.3 – 15.5	18.9 – 24.3

Table 4: Systematic uncertainties for the production cross sections in the medium  $z$  and low  $z$  regions. The error due to the  $J/\psi$  decay angular distribution does not apply to the polarisation analysis.

## 4 Results

Cross sections for  $ep \rightarrow eJ/\psi X$  are converted to  $\gamma p$  cross sections using the equivalent photon approximation [33, 34]. The photon proton cross section is defined by:

$$d\sigma_{ep} = \sigma_{\gamma p} f_{\gamma/e}(y) dy,$$

where  $f_{\gamma/e}$  denotes the photon flux<sup>5</sup> integrated over  $Q^2$  from the kinematic limit of  $Q_{min}^2$  to the upper limit of the measurement,  $Q_{max}^2 = 1 \text{ GeV}^2$ . The measured cross sections are given at the weighted mean for each bin assuming specific functional forms to fit the data, i.e.  $\sigma_{\gamma p}(W_{\gamma p}) \propto W_{\gamma p}^\delta$  and  $d\sigma/dp_{t,\psi}^2 \propto (p_{t,\psi}^2 + M_\psi^2)^{-n}$  as described below.

The measured cross sections are displayed in Figs. 4–9 and the numerical values are collected in Tables 8–11. In the next sections the measured cross sections are compared with theoretical calculations (Table 1).

### 4.1 Comparison of Cross sections with the Colour Singlet Model

The photon proton cross sections  $\sigma_{\gamma p}$ ,  $d\sigma/dz$  and  $d\sigma/dp_{t,\psi}^2$  in the medium  $z$  range are given in Figs. 4 and 5 and Table 8. The data are first compared with the NLO CSM calculations [21]. Although the  $p_{t,\psi}^2$  range of the measurement has been considerably enlarged compared with

<sup>5</sup> $f_{\gamma/e}(y) = \frac{\alpha}{2\pi} \left( 2m_e^2 y \left( \frac{1}{Q_{min}^2} - \frac{1}{Q_{max}^2} \right) + \frac{1+(1-y)^2}{y} \log \frac{Q_{max}^2}{Q_{min}^2} \right)$ , where  $Q_{min}^2 = m_e^2 \frac{y^2}{1-y}$ , taken from [34].

earlier analyses the agreement between data and theory remains good (Fig. 4c). The band on the theoretical calculations in Figs. 4 and 5 represents the uncertainties due to the variations of the mass of the charm quark,  $m_c = 1.4 \pm 0.1$  GeV and of  $\alpha_s(M_Z) = 0.1200 \pm 0.0025$  [26] (see Table 7 for the other parameter values). In the  $W_{\gamma p}$  and  $z$  distributions of Fig. 4a and b these uncertainties affect mainly the normalisation. The shapes and normalisations of the calculated cross sections as functions of  $W_{\gamma p}$  and  $z$  are in approximate agreement with the data for the two parameter sets,  $(m_c, \alpha_s) = (1.3 \text{ GeV}, 0.1175)$  and  $(1.4 \text{ GeV}, 0.1225)$ . The combinations  $m_c = 1.3 \text{ GeV}$  and  $\alpha_s(M_Z) = 0.1225$  (upper limit of the band) and  $m_c = 1.5 \text{ GeV}$  and  $\alpha_s(M_Z) = 0.1175$  (lower limit) can be excluded here.

The NLO CSM calculation describes the  $p_{t,\psi}^2$  distribution rather well (Fig. 4c). This is not the case for the LO CSM calculation, which lies above the data at low  $p_{t,\psi}^2$  and falls too steeply towards higher values of  $p_{t,\psi}^2$ . The  $p_{t,\psi}^2$  dependence is sensitive to the choice of  $m_c$  and  $\alpha_s$ . The calculations with  $(m_c, \alpha_s) = (1.3 \text{ GeV}, 0.1175)$  and  $(1.4 \text{ GeV}, 0.1225)$ , with which the  $W_{\gamma p}$  and  $z$  distributions are well described, also give a reasonable description of the  $p_{t,\psi}^2$  dependence apart from a tendency to undershoot the data at high  $p_{t,\psi}^2$ . The  $p_{t,\psi}^2$  distribution in bins of  $z$  (Fig. 5 and Table 9) is also described well by the NLO CSM calculation. This is interesting because the size of the colour octet contributions in the NRQCD approach is predicted to depend on  $z$ .

## 4.2 Parametrisations of Transverse Momentum Distributions

The differential cross sections  $d\sigma/dp_{t,\psi}^2 dz$  (Fig. 5 and Table 9) in the different  $z$  regions are found to be well described by a functional form  $(p_{t,\psi}^2 + M_\psi^2)^{-n}$ . Fits to the data have been performed and the results for the exponents  $n$  are summarised in Table 5. There is a tendency for  $n$  to decrease towards lower  $z$  values. A similar analysis has been carried out for inelastic  $J/\psi$  production in the range  $2 < Q^2 < 100 \text{ GeV}^2$  ( $0.3 < z < 0.9$ ,  $50 < W_{\gamma p} < 225 \text{ GeV}$ ) [1]. There the differential cross sections as a function of the transverse momentum in the photon proton center of mass system were fitted to the same functional form yielding a value  $n = 4.15 \pm 0.50$ , which agrees very well with the present result.

$W_{\gamma p}[\text{GeV}]$	$z$	$n$
60 – 240	0.3 – 0.9	$4.49 \pm 0.15$
60 – 240	0.75 – 0.90	$4.8 \pm 0.2$
	0.6 – 0.75	$4.6 \pm 0.2$
	0.3 – 0.6	$4.4 \pm 0.2$
120 – 260	0.05 – 0.45	$4.1 \pm 0.2$

Table 5: Results of fits to differential cross sections  $d\sigma/dp_{t,\psi}^2$  of the form  $(p_{t,\psi}^2 + M_\psi^2)^{-n}$  in different kinematic regions. Total experimental errors (statistical and systematic added in quadrature) have been used in the fits.

## 4.3 Comparison of Cross sections with NRQCD Calculations

The comparison of the measured cross sections  $d\sigma/dp_{t,\psi}^2$  and  $d\sigma/dz$  with the calculations within the NRQCD approach are shown in Figs. 6–8. For this comparison data in the low  $z$  region are

included (Tables 10 and 11). There are considerable uncertainties in such LO NRQCD calculations. The band in Figs. 6 and 7 gives an estimate from [21] of the main uncertainty, which arises from the LDMEs obtained from  $J/\psi$  production in  $p\bar{p}$  interactions. For the upper limit of the band the LDMEs extracted in LO are used, while for the lower limit values including estimates of higher orders in the extraction are used [12]. The distributions of  $p_{t,\psi}^2$  are shown in Fig. 6a and b for the low and medium  $z$  ranges, respectively. In both  $z$  regions the NRQCD calculation [21] and data are compatible within experimental and theoretical uncertainties. However there seems to be a difference in shape: the data have a slightly harder spectrum than predicted. For the low  $z$  range one should keep in mind that the calculation is for charm only, while the data contain feeddown from  $b$  quarks, which is expected to contribute a harder transverse momentum distribution. In both  $z$  regions the colour singlet contribution alone falls significantly faster than the data.

The differential cross section  $d\sigma/dz$  extending over the full  $z$  range,  $0.05 < z < 0.9$ , is compared with the same LO NRQCD calculation [21] in Fig. 7 for a cut  $p_{t,\psi}^2 > 1 \text{ GeV}^2$ . Resolved contributions are found to dominate in the calculation below  $z \lesssim 0.15$  (0.3) depending on the choice of LDMEs. In the comparison of data and theory one should note that the contribution from  $b$  decays in the data is sizeable at low  $z$  (of the order of 25%). Nevertheless one may infer from Fig. 7 that the LO NRQCD calculation, including CS and CO contributions, is able to give a fair description of the data both in shape and in normalisation, if the LDMEs are chosen to be close to the lowest available estimates (lower edge of the shaded band). Using larger LDME values in this calculation leads to a strong increase of the theoretical cross sections at high and low  $z$  values which is inconsistent with the measurements. The colour singlet contribution alone, which is also shown separately in Fig. 7, is roughly 30% below the data for  $z \gtrsim 0.5$  although the shape is adequately described in this region. At lower  $z$  values the colour singlet contribution falls below the data by up to a factor 3.

Although the uncertainties in the calculations are substantial, the measured cross section in the lowest  $z$  bin,  $0.05 < z < 0.15$ , suggests that a resolved photon contribution is present: Correcting for  $b$  and inelastic  $\psi(2S)$  feeddown using the estimates in Table 3 (section 3.4) and neglecting their uncertainties the measured cross section is found to be 2 standard deviations above the direct photon contributions alone (including CS and CO contributions with a range of LDME values as in Table 7 [21]).

A different calculation in the NRQCD framework has been carried out by Kniehl et al. [10] and is shown in Fig. 7 as 'HO improved'. In this calculation higher order effects were taken into account approximately using NLO parton density distributions for the photon and proton and using the LDMEs corrected for estimated higher orders effects (the parameters of the calculation are given in Table 7). This calculation gives a good description of the shape of the data but a normalisation factor of 3, as suggested by the authors [10], is necessary to reconcile the predicted cross section with the data.

The tendency for the colour octet contributions to rise towards high  $z$  values (upper end of shaded band in Fig. 7) is at variance with the data as has also been noted previously [2, 3]. This discrepancy may be due to phase space limitations at the upper limit of  $z$  where the emission of soft gluons in the conversion of the  $c\bar{c}$  pairs to  $J/\psi$  mesons is suppressed. This is not taken into account in [10, 21]. In [11] a resummation of the non-relativistic expansion was carried out, leading to a decrease of the predicted cross section at high  $z$ . In Fig. 8 (Table 8) the

measured cross sections  $d\sigma/dz$  for  $p_{t,\psi} > 2$  GeV and for  $p_{t,\psi} > 3$  GeV are compared with the results of these resummed calculations in the kinematic region of dataset I. The calculated curves have been roughly normalised to the data points at low  $z$ . The resummed calculation for  $\Lambda = 500$  MeV gives an acceptable description of the data<sup>6</sup> at  $p_{t,\psi} > 3$  GeV while the agreement between data and calculation is still poor for  $p_{t,\psi} > 2$  GeV or for lower  $\Lambda$  values.

#### 4.4 Comparison of Cross sections with $k_t$ Factorisation Calculations

An entirely different approach to inelastic  $J/\psi$  production within the CSM [16] is implemented in the Monte Carlo program CASCADE [15]. Here direct photon gluon fusion processes are computed in the  $k_t$  factorisation approach [17, 18] using an unintegrated ( $k_t$  dependent) gluon density in the proton and the gluons may thus be off-shell. This gluon density was obtained from a fit [15] to the HERA structure function data (using the CCFM parton evolution equations). Fig. 9 shows a comparison of the data with the results from CASCADE. In Fig. 9a  $d\sigma/dz$  is shown as a function of  $z$ . Good agreement is observed between data and predictions for  $z \lesssim 0.8$ . At high  $z$  values the CASCADE calculation underestimates the cross section. This may be due to missing relativistic corrections which are not available for the off-shell matrix element. It could also indicate a possible missing CO contribution. The  $W_{\gamma p}$  distribution is shown for the restricted  $z$  range  $0.3 < z < 0.8$  (Fig. 9b) and the CASCADE model is found to be in reasonable agreement with the data. An important improvement compared to collinear LO calculations is visible in the  $p_{t,\psi}^2$  dependence (for  $0.3 < z < 0.9$ , Fig. 9c), where the CASCADE predictions fit the data quite well. This is due to the transverse momentum of the gluons from the proton which contributes to the transverse momentum of the  $J/\psi$  meson.

#### 4.5 Polarisation Measurement

The polarisation of the  $J/\psi$  meson is expected to differ in the various theoretical approaches discussed here and could in principle be used to distinguish between them, independently of normalisation uncertainties. The polarisation analysis is performed in the ‘‘target frame’’, the rest system of the  $J/\psi$  meson, using the direction opposite to that of the incoming proton as reference axis  $z'$ . Two angles are defined:  $\theta^*$  is the polar angle of the positive decay muon with respect to the  $z'$  axis and  $\Phi^*$  is the angle between the plane of the decay muons and the plane defined by the photon and the  $z'$ -axis.

The corrected data in the medium  $z$  range (dataset I) are normalised to the integrated cross sections and fitted to the forms [19]:

$$\frac{1}{\sigma} \frac{d\sigma}{d \cos \theta^*} \propto 1 + \lambda \cos^2 \theta^* ; \quad (1)$$

$$\frac{1}{\sigma} \frac{d\sigma}{d\Phi^*} \propto 1 + \frac{\lambda}{3} + \frac{\nu}{3} \cos 2\Phi^* . \quad (2)$$

---

<sup>6</sup>The parameter  $\Lambda$  describes the energy lost by the  $c\bar{c}$  system, in its rest system, in the conversion to the  $J/\psi$  meson.

$z$ interval	$\lambda$	$\nu$
0.3 – 0.6	$1.1 \pm 0.4$	$-0.2 \pm 0.5$
0.6 – 0.75	$0.6 \pm 0.4$	$-0.4 \pm 0.5$
0.75 – 0.9	$0.1 \pm 0.4$	$-0.6 \pm 0.4$
$p_{t,\psi}$ interval [ GeV]	$\lambda$	$\nu$
1 – 2	$1.3 \pm 0.5$	$-0.3 \pm 0.5$
2 – 3	$0.6 \pm 0.5$	$-0.3 \pm 0.5$
> 3	$0.1 \pm 0.4$	$-0.3 \pm 0.4$

Table 6: Fit results for the polarisation parameters  $\lambda$  and  $\nu$  as functions of  $z$  and  $p_{t,\psi}$ . The errors are due to the total experimental uncertainties.

The parameters  $\lambda$  and  $\nu$  can be related to the polarisation of the  $J/\psi$  meson. The cases  $\lambda = 1$  and  $-1$  correspond to transverse and longitudinal polarisation of the  $J/\psi$  meson, respectively. Fits of the data to equations (1) and (2) are performed in 3 bins of  $z$  or in 3 bins of  $p_{t,\psi}$ . The polar angular distribution in  $z$  bins is shown as an example in Fig. 10. The results for  $\lambda$  are listed in table 6 and plotted in Fig. 11a and c. Positive values are preferred although a decrease is observed with increasing  $z$  and increasing  $p_{t,\psi}$ . The fit of the  $\Phi^*$  distribution is also performed in  $z$  and  $p_{t,\psi}$  bins using the fitted values for  $\lambda$ . The resulting  $\nu$  values are slightly negative (see Table 6 and Fig. 11b and d) and within errors independent of  $z$  and  $p_{t,\psi}$ .

In Fig. 11 the results for three LO calculations are shown together with the data: the NRQCD prediction including colour octet and colour singlet contributions [19], the colour singlet contribution alone and a calculation using a  $k_t$  factorisation approach and off-shell gluons [20]. The errors in the data preclude any firm conclusions. None of the three calculations predicts a decrease of  $\lambda$  with increasing  $z$ , while a decrease with increasing  $p_{t,\psi}$  as observed in the data is expected for the  $k_t$  factorisation ansatz. The full NRQCD prediction is also compatible with this. In order to distinguish between full NRQCD and the colour singlet contribution alone, measurements at larger  $p_{t,\psi}$  are required. The measured values of  $\nu$ , for which no prediction is available from the  $k_t$  factorisation approach, favour the full NRQCD prediction.

## 5 Summary and Conclusions

An analysis of inelastic photoproduction of  $J/\psi$  mesons is presented. The kinematic region covers  $60 < W_{\gamma p} < 260$  GeV,  $p_{t,\psi}^2 > 1$  GeV<sup>2</sup> and  $0.05 < z < 0.9$ . Cross sections in the low  $z$  region,  $z \lesssim 0.3$ , are presented for the first time. The data can be described by boson gluon fusion calculations. In the low  $z$  range the agreement between data and (LO) calculations is improved by including resolved photon processes although the uncertainties due to contributions from  $b$  decays are appreciable in this region. The differential cross sections are compared with calculations in three different theoretical frameworks.

Firstly, in the medium  $z$  range,  $0.3 \leq z \leq 0.9$ , (double) differential cross sections are compared with calculations in the Colour Singlet Model (CSM) in NLO for direct photons. These are found to give a good description of the distributions in  $W_{\gamma p}$ ,  $z$  and  $p_{t,\psi}^2$  (tested up to a value of

$p_{t,\psi}^2 \sim 60 \text{ GeV}^2$ ). The NLO calculations show a hard  $p_t$  spectrum which describes the data well in contrast to the LO calculation. The distribution of the transverse momentum of the  $J/\psi$  is also found to be well described in three separate regions of  $z$ . The estimated theoretical uncertainties due to the uncertainties in the charm mass and  $\alpha_s$  are much larger than the experimental errors, so the data may be used to constrain parameters of the model.

A second comparison in this medium  $z$  range is made with a LO calculation within the CSM, allowing the interacting gluons to have transverse momentum ( $k_t$  factorisation approach). This Monte Carlo calculation is also found to give a good description of the data.

The third comparison in the whole  $z$  range ( $0.05 < z < 0.9$ ) involves LO non-relativistic QCD calculations (NRQCD) including colour octet as well as colour singlet contributions. This is of importance since the Colour Singlet Model (in LO) does not describe charmonium production in  $p\bar{p}$  collisions and has fundamental theoretical problems in the description of  $p$ -wave states. The present differential cross sections can be reasonably well described in shape by the NRQCD calculations when including direct and resolved contributions. The normalisation depends on the details of the calculations, in particular on the chosen octet long distance matrix elements (LDMEs). The present photoproduction data clearly favour very low values of the octet LDMEs. At high  $z$ , resummed NRQCD calculations applicable at large  $p_{t,\psi}$ , tend to improve the agreement with the data. At low  $z$  the inclusion of colour octet contributions improves the agreement between data and theory. However, decays of  $b$  flavoured hadrons are expected to play an important role here and are neglected in the present analysis.

The  $p_{t,\psi}^2$  distribution is reasonably reproduced by the NRQCD calculation, which however gives a slightly softer  $p_{t,\psi}^2$  dependence than that measured in the medium and in the low  $z$  ranges. Including NLO effects would probably improve the agreement with the measurements as already seen in the CSM.

The polarisation parameters of the  $J/\psi$  meson have been measured as a function of  $p_{t,\psi}$  and  $z$ . Within present experimental and theoretical errors NRQCD, the CSM and the  $k_t$  factorisation approach all fit the data reasonably well.

With an appropriate choice of parameters, theoretical calculations within the NRQCD approach, constrained by results from  $p\bar{p}$  collisions can describe the present photoproduction measurements. Next-to-leading order corrections are likely to improve the agreement even after colour octet contributions are included. The data have the potential to reduce the current large uncertainties in the phenomenological parameters. This contributes to the development of a unified understanding of charmonium production in different environments such as  $p\bar{p}$ ,  $ep$  and  $\gamma p$  collisions.

## Acknowledgements

We are grateful to the HERA machine group whose outstanding efforts have made and continue to make this experiment possible. We thank the engineers and technicians for their work in constructing and now maintaining the H1 detector, our funding agencies for financial support, the DESY technical staff for continual assistance, and the DESY directorate for the hospitality which they extend to the non DESY members of the collaboration. We want to thank M. Krämer for close collaboration and S. Wolf, B.A. Kniehl and S.P. Baranov for many discussions and for making their theoretical calculations available to us.

## References

- [1] C. Adloff *et al.* [H1 Coll.], “Inelastic Leptoproduction of  $J/\psi$  Mesons at HERA”, DESY 02-060, submitted to Eur. Phys. J. C
- [2] S. Aid *et al.* [H1 Coll.], Nucl. Phys. B **472** (1996) 3 [hep-ex/9603005].
- [3] J. Breitweg *et al.* [ZEUS Coll.], Z. Phys. C **76** (1997) 599 [hep-ex/9708010].
- [4] J. Breitweg *et al.* [ZEUS Coll.], Z. Phys. C **75**, (1997) 215 [hep-ex/9704013];  
C. Adloff *et al.* [H1 Coll.], Phys. Lett. B **483**, (2000) 23 [hep-ex/0003020];  
S. Chekanov *et al.* [ZEUS Coll.], accepted by Eur. Phys. J. C [hep-ex/0201043].
- [5] E. L. Berger and D. L. Jones, Phys. Rev. D **23** (1981) 1521;  
R. Baier and R. Rückl, Phys. Lett. B **102** (1981) 364; Z. Phys. C **19** (1983) 251;  
Nucl. Phys. B **201** (1982) 1.
- [6] F. Halzen, Phys. Lett. B **69** (1977) 105;  
O. J. Eboli, E. M. Gregores and F. Halzen, Phys. Lett. B **451** (1999) 241 [hep-ph/9802421].
- [7] A. Edin, G. Ingelman and J. Rathsman, Phys. Rev. D **56** (1997) 7317 [hep-ph/9705311].
- [8] G. T. Bodwin, E. Braaten and G. P. Lepage, Phys. Rev. D **51** (1995) 1125;  
[Erratum-ibid. D **55** (1995) 5853] [hep-ph/9407339];  
E. Braaten and Y. Q. Chen, Phys. Rev. D **54** (1996) 3216 [hep-ph/9604237];  
W. E. Caswell and G. P. Lepage, Phys. Lett. B **167** (1986) 437.
- [9] F. Abe *et al.* [CDF Coll.], Phys. Rev. Lett. **79** (1997) 572; *ibid.* **79** (1997) 578.
- [10] B. A. Kniehl and G. Kramer, Eur. Phys. J. C **6** (1999) 493 [hep-ph/9803256].
- [11] M. Beneke, G. A. Schuler and S. Wolf, Phys. Rev. D **62** (2000) 034004 [hep-ph/0001062].
- [12] B. Cano-Coloma and M. A. Sanchis-Lozano, Nucl. Phys. B **508** (1997) 753 [hep-ph/9706270].
- [13] K. Sridhar, A. D. Martin and W. J. Stirling, Phys. Lett. B **438** (1998) 211 [hep-ph/9806253].
- [14] M. Krämer, Nucl. Phys. B **459** (1996) 3 [hep-ph/9508409].
- [15] H. Jung and G. P. Salam, Eur. Phys. J. C **19** (2001) 351 [hep-ph/0012143]; H. Jung, hep-ph/0109102.
- [16] V. A. Saleev and N. P. Zotov, Mod. Phys. Lett. A **9** (1994) 151;  
[Erratum-*ibid.* A **9** (1994) 1517].
- [17] S. Catani, M. Ciafaloni and F. Hautmann, Nucl. Phys. B **366** (1991) 135
- [18] J. C. Collins and R. K. Ellis, Nucl. Phys. B **360** (1991) 3.
- [19] M. Beneke, M. Krämer and M. Vanttinen, Phys. Rev. D **57** (1998) 4258 [hep-ph/9709376]

- [20] S. P. Baranov, Phys. Lett. B **428** (1998) 377.
- [21] M. Krämer, Prog. Part. Nucl. Phys. **47** (2001) 141 [hep-ph/0106120].
- [22] C. Adloff *et al.* [H1 Coll.], Eur. Phys. J. C **10** (1999) 373 [hep-ex/9903008].
- [23] I. Abt *et al.* [H1 Coll.], Nucl. Instrum. Meth. A **386** (1997) 310; *ibid.* **A386** (1997) 348.
- [24] K. Krüger, “Photoproduction of  $J/\psi$  mesons at medium and low elasticities at HERA,” PhD thesis, DESY-THESIS-2001-025, also at [http://www-h1.desy.de/publications/theses\\_list.html](http://www-h1.desy.de/publications/theses_list.html).
- [25] F. Jacquet, A. Blondel, Proceedings of the workshop: Study for an ep facility in Europe, DESY 79-048 (1979) 391
- [26] D. E. Groom *et al.* [Particle Data Group Coll.], Eur. Phys. J. C **15** (2000) 1.
- [27] H. Jung, in: Proc. of the Workshop on Physics at HERA, ed. W. Buchmüller and G. Ingelman, Hamburg (1992), Vol. 3, p. 1488;  
H. Jung, D. Krücker, C. Greub and D. Wyler, Z. Phys. C **60** (1993) 721.
- [28] A. D. Martin, W. J. Stirling and R. G. Roberts, Phys. Lett. B **354** (1995) 155 [hep-ph/9502336].
- [29] M. Glück, E. Reya and A. Vogt, Phys. Rev. D **46** (1992) 1973; Phys. Rev. D **45** (1992) 3986; Z. Phys. C **67** (1995) 433.
- [30] G. Ingelman, J. Rathsman and G. A. Schuler, Comput. Phys. Commun. **101** (1997) 135 [hep-ph/9605285].
- [31] C. Adloff *et al.* [H1 Coll.], Phys. Lett. B **467** (1999) 156; [Erratum-*ibid.* B **518** (1999) 331] [hep-ex/9909029].
- [32] B. List and A. Mastroberardino, in: Proc. of the Workshop on Monte Carlo generators for HERA physics, ed. A. T. Doyle *et al.*, DESY-PROC-1999-02 (1999) 396.
- [33] C. F. von Weizsäcker, Z. Phys. **88** (1934) 612;  
E. J. Williams, Phys. Rev. **45** (1934) 729;  
V. M. Budnev *et al.*, Phys. Rept. **15** (1974) 181.
- [34] S. Frixione, M. L. Mangano, P. Nason and G. Ridolfi, Phys. Lett. B **319** (1993) 339 [hep-ph/9310350].
- [35] A. D. Martin, R. G. Roberts, W. J. Stirling and R. S. Thorne, Eur. Phys. J. C **4** (1998) 463 [hep-ph/9803445].
- [36] H. L. Lai *et al.* [CTEQ Coll.], Eur. Phys. J. C **12** (2000) 375 [hep-ph/9903282].
- [37] G. T. Bodwin, E. Braaten and G. P. Lepage, Phys. Rev. D **46** (1992) 1914 [hep-lat/9205006].

Parameters NLO CSM (M. Krämer [14])	Figures 4 and 5
PDF	MRST [35]
Renormalisation/Factorisation scale	$\sqrt{2} m_c, \max[\sqrt{2} m_c, 1/2 \sqrt{m_c^2 + p_t^2}]$ (for $p_{t,\psi}^2$ )
$\langle \mathcal{O}[1, {}^3S_1] \rangle$	$1.16 \text{ GeV}^3$
$m_c$	$1.3 \leq m_c \leq 1.5 \text{ GeV}$
$\alpha_s(M_Z)$	$0.1200 \pm 0.0025$
Parameters NRQCD (M. Krämer [21])	Figures 6 and 7
PDF	GRV(LO) [29] for proton and photon
$\Lambda_{LO}^{(4)}$	200 MeV
Renormalisation/Factorisation scale	$2 m_c$
$m_c$	1.5 GeV
$\langle \mathcal{O}[1, {}^3S_1] \rangle$	$1.16 \text{ GeV}^3$
$\langle \mathcal{O}[8, {}^3S_1] \rangle$	$(0.3 - 2.0) \cdot 10^{-2} \text{ GeV}^3$
$\langle \mathcal{O}[8, {}^1S_0] \rangle + 3.5 \langle \mathcal{O}[8, {}^3P_0] \rangle / m_c^2$	$(1.0 - 10) \cdot 10^{-2} \text{ GeV}^3$
Resummed calculations (Beneke et al. [11])	Figure 8
$\langle \mathcal{O}[8, {}^1S_0] \rangle + 3.1 \langle \mathcal{O}[8, {}^3P_0] \rangle / m_c^2$	$1.5 \cdot 10^{-2} \text{ GeV}^3$
$\langle \mathcal{O}[8, {}^3S_1] \rangle$	$(0.5 - 1.0) \cdot 10^{-2} \text{ GeV}^3$
other parameters as in the NRQCD calculation [21]	
Parameters NRQCD (Kniehl et al. [10])	Figure 7
PDF	CTEQ5M [36] / GRV-HO for proton and photon
$\Lambda_{\overline{MS}}^{(4)}$	326 MeV
Renormalisation/Factorisation scale	$\sqrt{4 m_c^2 + p_t^2}$
$m_c$	$M_\psi / 2$
$\langle \mathcal{O}[1, {}^3S_1] \rangle$	$(1.3 \pm 0.09) \text{ GeV}^3$
$\langle \mathcal{O}[8, {}^1S_0] \rangle + 3.54 \langle \mathcal{O}[8, {}^3P_0] \rangle / m_c^2$	$(0.572 \pm 0.184) \cdot 10^{-2} \text{ GeV}^3$
$\langle \mathcal{O}[8, {}^3S_1] \rangle$	$(0.273 \pm 0.045) \cdot 10^{-2} \text{ GeV}^3$

Table 7: Parameters used in the QCD calculations which are compared to the data. The expressions “ $\langle \mathcal{O}[8, {}^3S_1] \rangle$ ” etc. denote the long distance matrix elements. The colour octet LDMEs are extracted from high  $p_t$   $J/\psi$  production in  $p\bar{p}$  collisions for the NRQCD calculations of [10, 21] and from data on  $B$  decays in [11]. For more details and for a discussion of the uncertainties see these references.

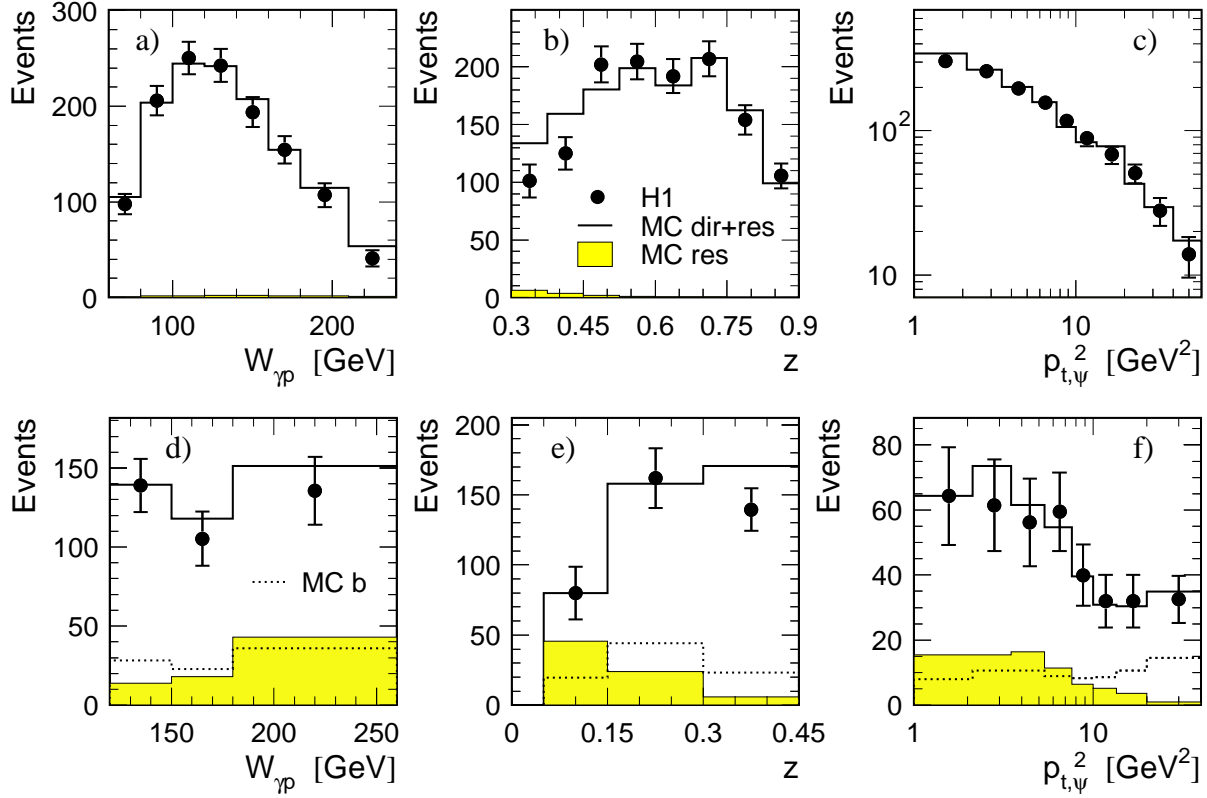


Figure 3: Comparison between data and Monte Carlo simulations after all selection cuts and after subtraction of non-resonant background. a)  $W_{\gamma p}$ , b)  $z$  and c)  $p_{t,\psi}^2$  distributions in the range  $0.3 < z < 0.9$ ,  $60 < W_{\gamma p} < 240$  GeV and  $p_{t,\psi}^2 > 1$  GeV<sup>2</sup> (dataset I). d)  $W_{\gamma p}$ , e)  $z$  and f)  $p_{t,\psi}^2$  distributions in the range  $0.05 < z < 0.45$ ,  $120 < W_{\gamma p} < 260$  GeV and  $p_{t,\psi}^2 > 1$  GeV<sup>2</sup> (dataset II). The error bars on the data points are statistical only. The EPJPSI simulation of direct + resolved photon processes (full histograms) and resolved photon processes (shaded histograms) are compared with the data (for the relative normalisation see text). An estimate of the direct photon contribution from  $b \rightarrow J/\psi + X$  from EPJPSI (which is not included in the full histogram) is also shown as a dotted histogram in d)–f).

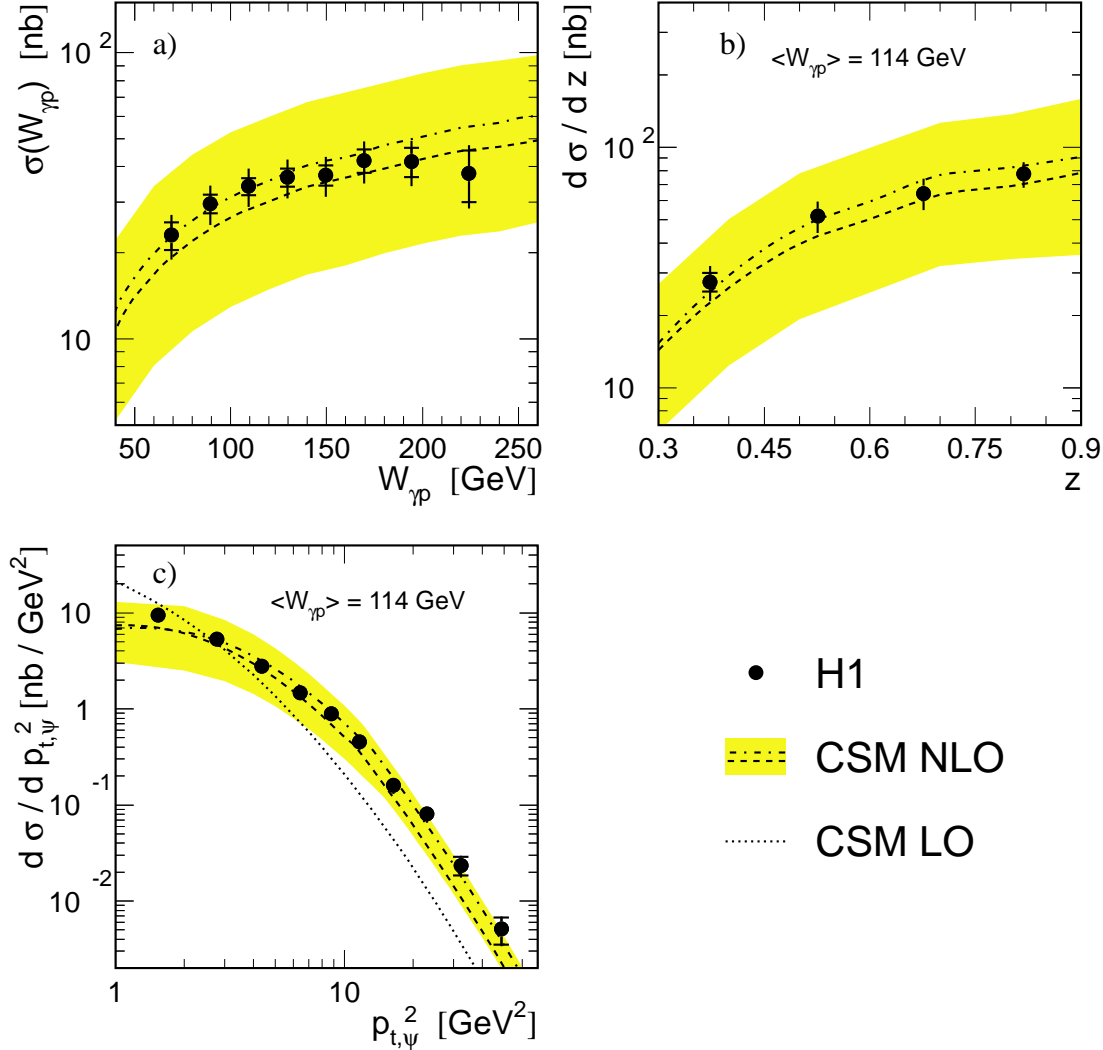


Figure 4: *Inelastic  $J/\psi$  production in the region  $60 < W_{\gamma p} < 240$  GeV,  $0.3 < z < 0.9$  and  $p_{t,\psi}^2 > 1$  GeV<sup>2</sup>. a) Total cross section as a function of  $W_{\gamma p}$ , b) differential cross sections  $d\sigma/dz$  and c)  $d\sigma/dp_{t,\psi}^2$ . The H1 data are shown together with NLO calculations in the Colour Singlet Model [14] with MRST [35] parton density functions ( $W_{\gamma p} = 115$  GeV for b) and c)). The shaded band reflects the uncertainties in  $m_c$  and  $\alpha_s$  (see Table 7); the dashed (dash-dotted) curve is calculated with  $m_c = 1.3(1.4)$  GeV,  $\alpha_s(M_Z) = 0.1175(0.1225)$ . In c) a CSM LO calculation with MRST parton distributions,  $m_c = 1.3$  GeV,  $\alpha_s(M_Z) = 0.1225$  is also shown (dotted).*

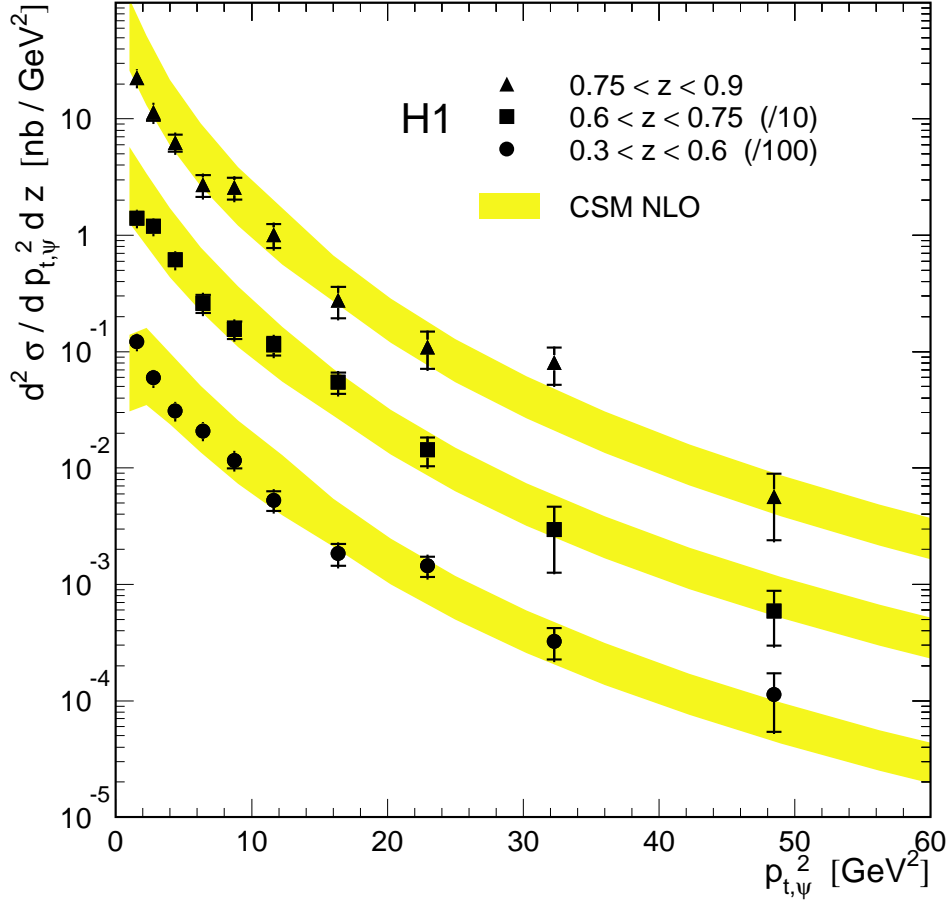


Figure 5: Double differential cross section  $d^2\sigma/dp_{t,\psi}^2 dz$  in the same kinematic region and compared with the same CSM NLO calculations as in Fig. 4.

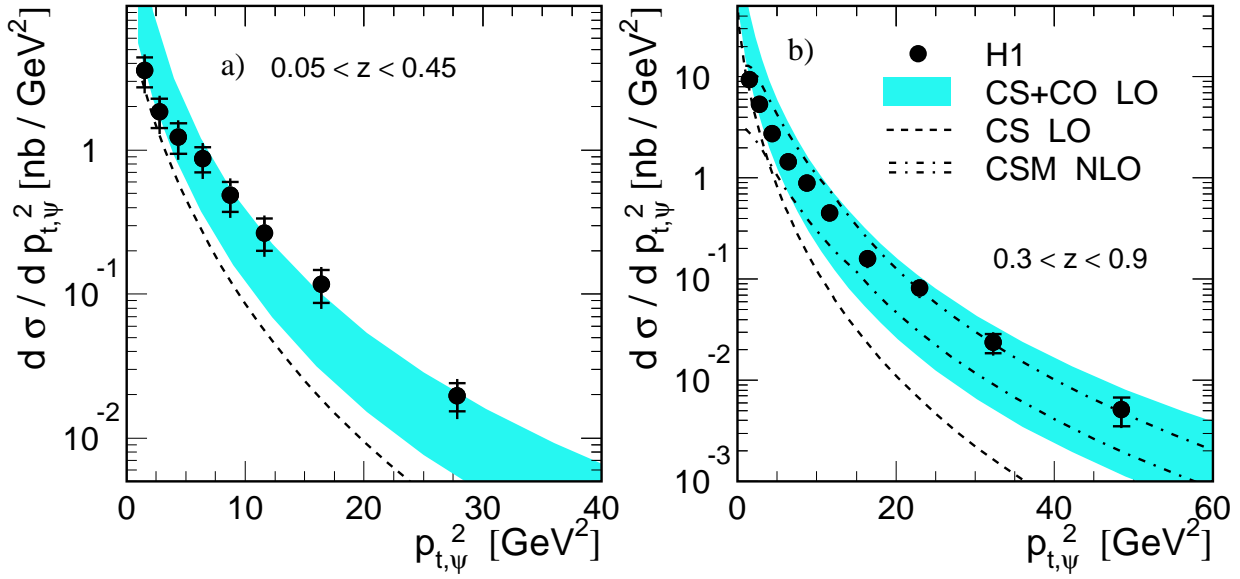


Figure 6: *Differential cross section  $d\sigma/dp_{t,\psi}^2$  for inelastic  $J/\psi$  production in two kinematic regions. a)  $0.05 < z < 0.45$ ,  $120 < W_{\gamma p} < 260 \text{ GeV}$ ; b)  $0.3 < z < 0.9$ ,  $60 < W_{\gamma p} < 240 \text{ GeV}$  (same data as in Fig. 4c). The data are compared with LO theoretical calculations in the NRQCD framework, including colour octet and colour singlet contributions from direct and resolved photons shown as the shaded band, which reflects the uncertainties due to the LDMEs. The dashed line shows the colour singlet contribution separately. In b) the band of the same CSM NLO calculation [14] as in Fig. 4c is also shown as dash-dotted lines.*

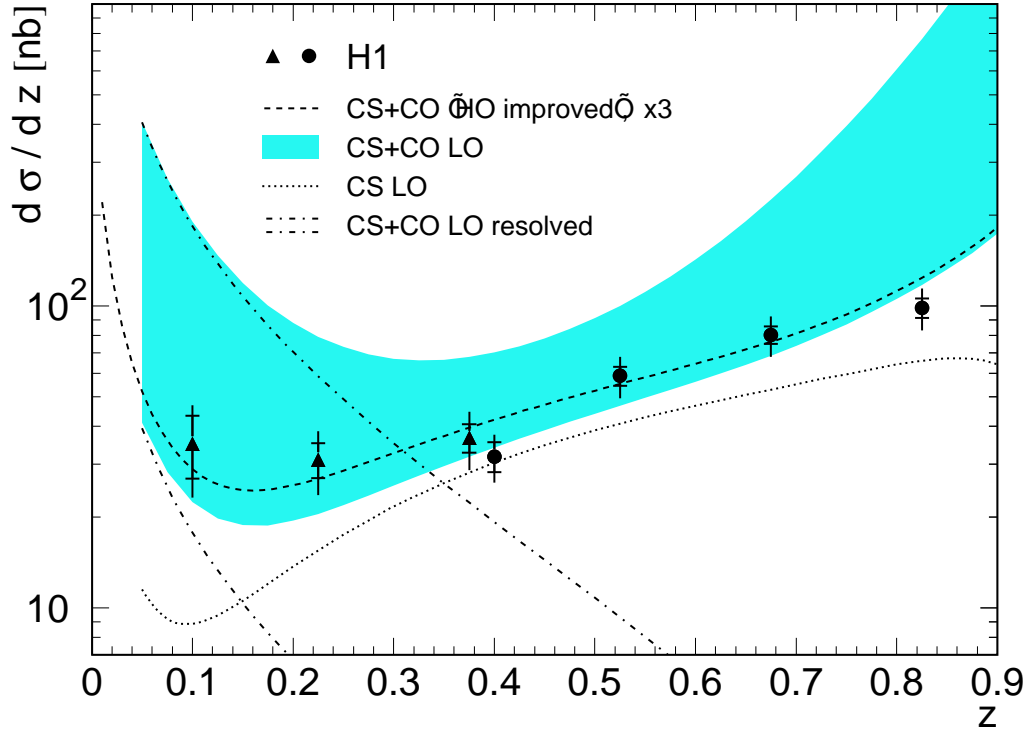


Figure 7: Differential cross section  $d\sigma/dz$  for  $120 < W_{\gamma p} < 260$  GeV and  $p_{t,\psi}^2 > 1$  GeV. The data are shown as triangles (points) corresponding to datasets II (III). The two data points from different analyses at  $z \approx 0.4$  are statistically correlated and offset for visibility. Theoretical calculations within the NRQCD/factorisation framework including colour octet and colour singlet contributions from direct and resolved photons are shown for comparison. The shaded band is a calculation by Krämer [21] reflecting the uncertainties due to the LDMEs (see Table 7). The two dash-dotted lines indicate the region of the resolved contributions (CS+CO) separately and the dotted line shows the colour singlet contribution. The dashed line is the result of a NRQCD calculation by Kniehl et al. [10], where higher order effects have been estimated and which has been normalised to the data. Note that the theoretical calculations are for charm only, while the data contain a residual background from  $b$  quarks at low  $z$ .

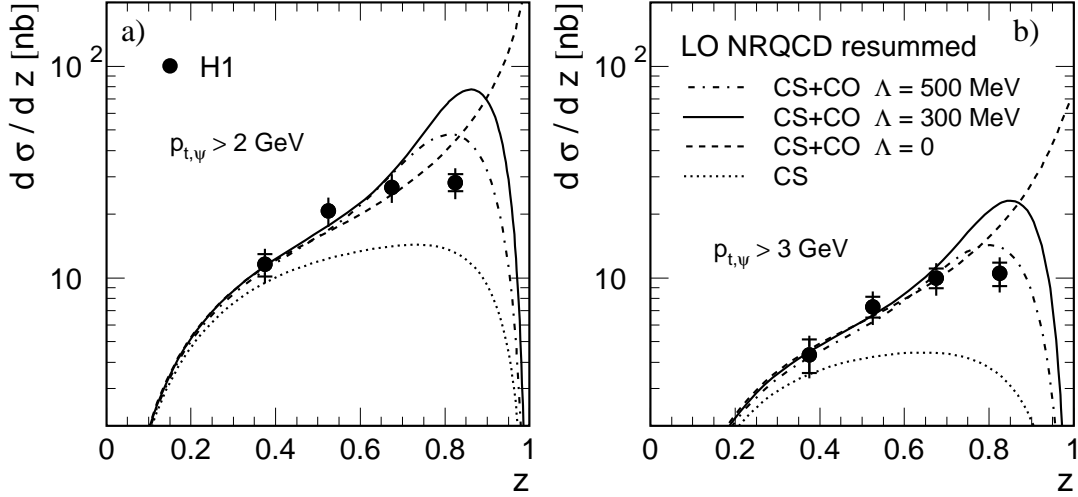


Figure 8: *Differential cross sections  $d\sigma/dz$  ( $60 < W_{\gamma p} < 240$  GeV) for a)  $p_{t,\psi} > 2$  GeV and b)  $p_{t,\psi} > 3$  GeV in comparison with NRQCD calculations including colour octet and colour singlet contributions after resumming soft contributions at high  $z$  [11]. The curves correspond to three values of the parameter  $\Lambda = 0$  (no resummation), 300 and 500 MeV (dashed, full and dash-dotted lines). The dotted line is the colour singlet contribution alone. The theoretical curves have been scaled with a common factor 2 in a) and 3 in b), respectively.*

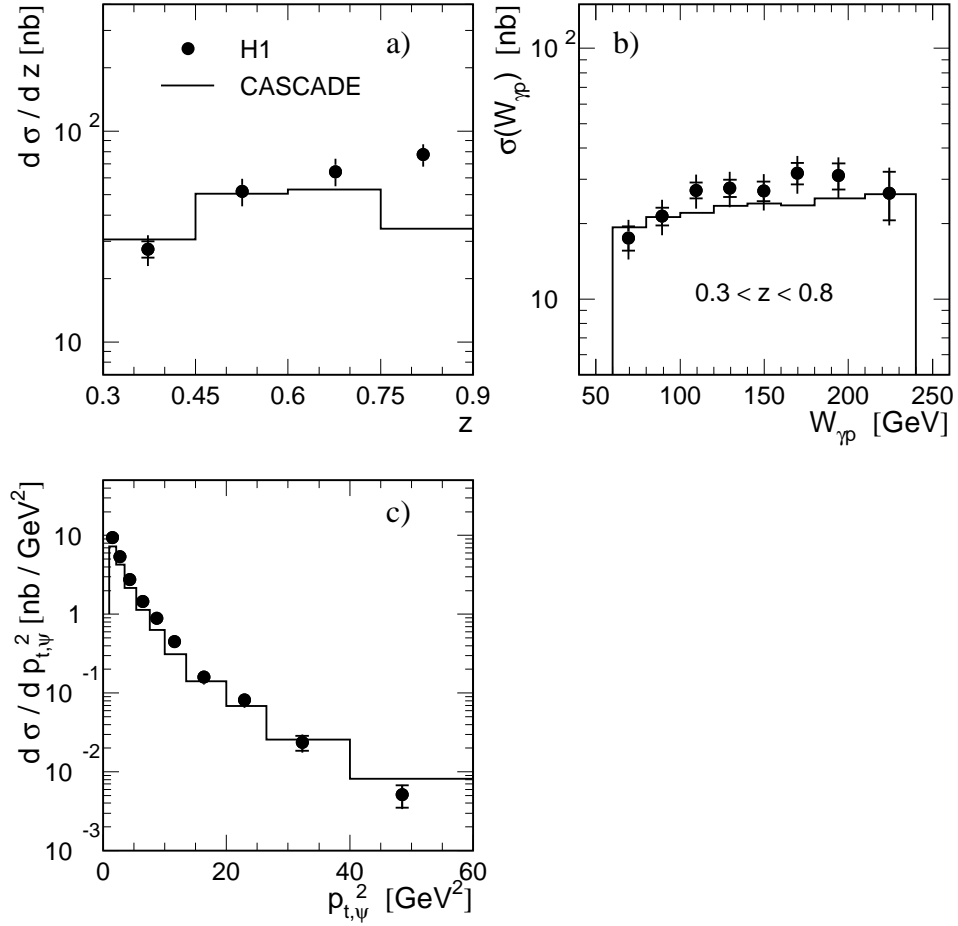


Figure 9: *Inelastic  $J/\psi$  production in the region  $60 < W_{\gamma p} < 240$  GeV,  $0.3 < z < 0.9$  and  $p_{t,\psi}^2 > 1$  GeV $^2$  in comparison with a  $k_t$  factorisation model implemented in the Monte Carlo generator CASCADE [15]. a) Differential cross section  $d\sigma/dz$ , b)  $\sigma_{\gamma p}$  as a function of  $W_{\gamma p}$  for  $0.3 < z < 0.8$  and c)  $d\sigma/dp_{t,\psi}^2$ .*

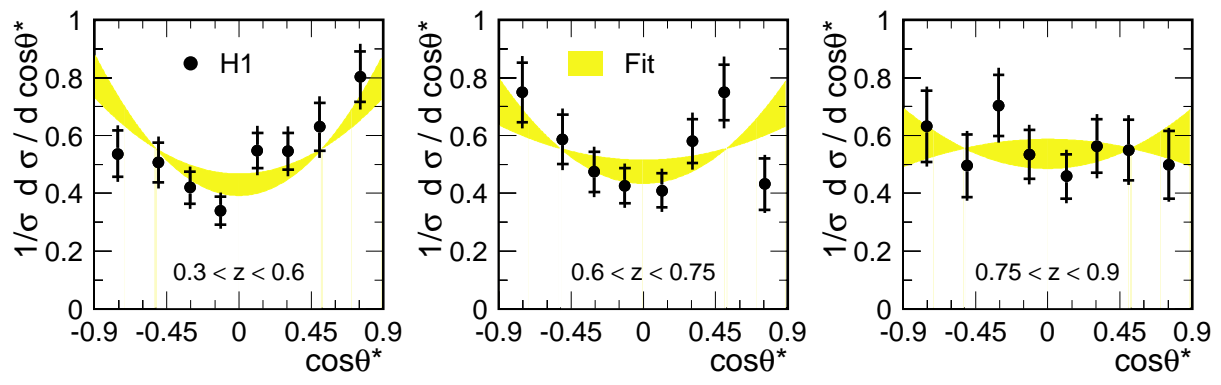


Figure 10: *Differential cross sections  $1/\sigma d\sigma/d\cos\theta^*$  in the rest system of the  $J/\psi$  meson for different  $z$  regions (kinematic region  $60 < W < 240$  GeV,  $p_{t,\psi}^2 > 1$  GeV<sup>2</sup>) normalised for  $|\cos\theta^*| < 0.9$ . The inner error bars indicate the statistical uncertainty, while the outer error bars include the statistical and systematic uncertainties added in quadrature. The shaded bands reflect fits to the form  $\sim 1 + \lambda \cos^2 \theta^*$ . The contours of  $\pm 1$  standard deviation are shown.*

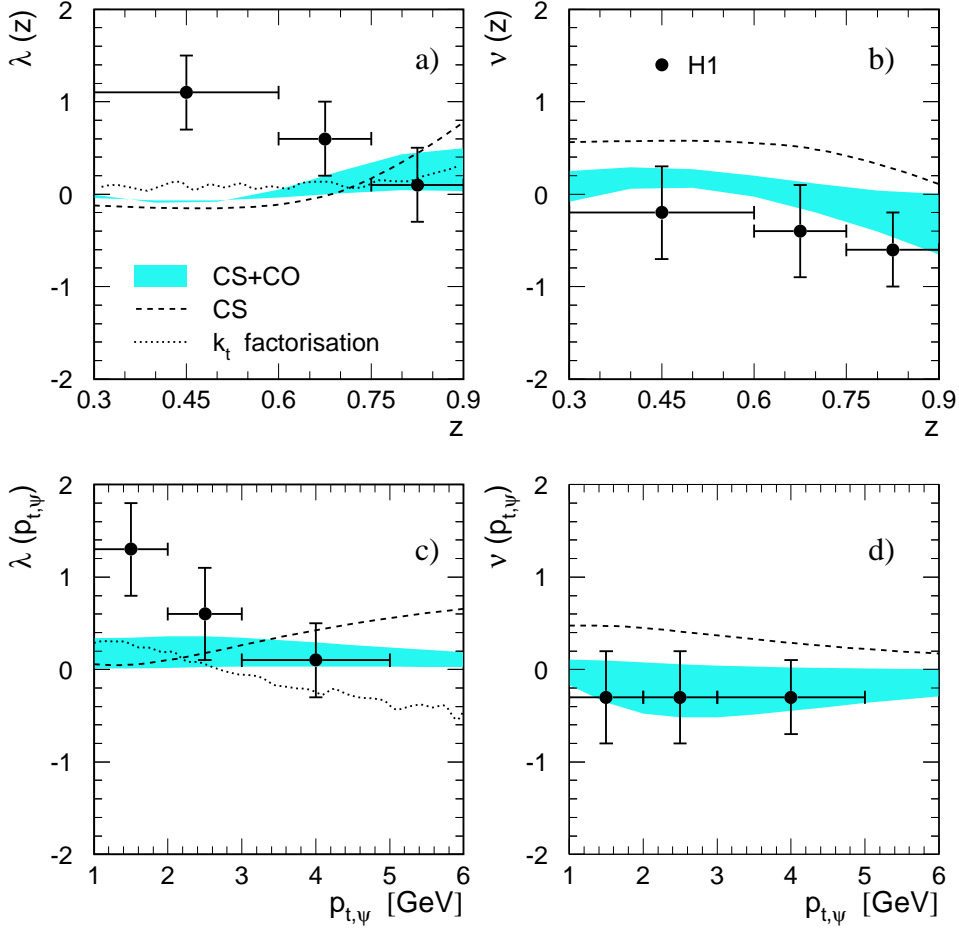


Figure 11: *Polarisation parameters  $\lambda$  (a and c) and  $\nu$  (b and d) in the target frame as functions of  $z$  (a and b) and  $p_{t,\psi}$  (c and d). The error bars on the data points correspond to the total experimental error. The theoretical calculations shown are from the NRQCD approach [19] (shaded bands) with colour octet and colour singlet contributions, while the dashed curves show the result from the colour singlet contribution separately. For  $\lambda$  a calculation within the  $k_t$  factorisation approach [20] is also shown (dotted line).*

$W_{\gamma p}$ [GeV]	$\langle W_{\gamma p} \rangle$	$\sigma_{\gamma p}$ [nb]	
		$0.3 < z < 0.9$	$0.3 < z < 0.8$
60 – 80	69.3	$23.0 \pm 2.5 \pm 3.2$	$17.5 \pm 2.0 \pm 2.4$
80 – 100	89.4	$29.7 \pm 2.2 \pm 4.1$	$21.4 \pm 1.7 \pm 3.0$
100 – 120	109.5	$34.1 \pm 2.3 \pm 4.7$	$27.2 \pm 2.0 \pm 3.8$
120 – 140	129.6	$36.7 \pm 2.6 \pm 5.1$	$27.7 \pm 2.2 \pm 3.9$
140 – 160	149.6	$37.3 \pm 3.0 \pm 5.2$	$27.0 \pm 2.4 \pm 3.8$
160 – 180	169.6	$42.0 \pm 3.9 \pm 5.8$	$31.8 \pm 3.1 \pm 4.4$
180 – 210	194.2	$41.7 \pm 4.9 \pm 5.8$	$31.1 \pm 3.7 \pm 4.3$
210 – 240	224.2	$37.8 \pm 7.8$ $+5.9$ $-5.0$	$26.4 \pm 5.8$ $+4.1$ $-3.5$

$z$	$\langle z \rangle$	$d\sigma_{\gamma p}/dz$ [nb]		
		$p_{t,\psi} > 1$ GeV	$p_{t,\psi} > 2$ GeV	$p_{t,\psi} > 3$ GeV
0.30 – 0.45	0.38	$27.5 \pm 2.4 \pm 3.8$	$11.6 \pm 1.4 \pm 1.6$	$4.3 \pm 0.8 \pm 0.6$
0.45 – 0.60	0.53	$51.7 \pm 2.8 \pm 7.2$	$20.8 \pm 1.6 \pm 2.9$	$7.3 \pm 0.8 \pm 1.0$
0.60 – 0.75	0.68	$64.3 \pm 3.4 \pm 8.9$	$26.8 \pm 2.0 \pm 3.7$	$10.0 \pm 1.1 \pm 1.4$
0.75 – 0.90	0.83	$77.4 \pm 5.0 \pm 10.8$	$28.3 \pm 2.6 \pm 3.9$	$10.5 \pm 1.3 \pm 1.5$

$p_{t,\psi}^2$ [GeV <sup>2</sup> ]	$\langle p_{t,\psi}^2 \rangle$	$d\sigma_{\gamma p}/dp_{t,\psi}^2$ [nb/GeV <sup>2</sup> ]
1.0 – 2.1	1.54	$9.45 \pm 0.61 \pm 1.31$
2.1 – 3.5	2.78	$5.34 \pm 0.37 \pm 0.74$
3.5 – 5.4	4.38	$2.77 \pm 0.22 \pm 0.38$
5.4 – 7.6	6.43	$1.46 \pm 0.13 \pm 0.20$
7.6 – 10.0	8.74	$0.887 \pm 0.088 \pm 0.123$
10.0 – 13.5	11.6	$0.452 \pm 0.053 \pm 0.063$
13.5 – 20.0	16.4	$0.160 \pm 0.022 \pm 0.022$
20.0 – 26.5	23.0	$0.0815 \pm 0.0120 \pm 0.0113$
26.5 – 40.0	32.3	$0.0236 \pm 0.0051 \pm 0.0033$
40.0 – 60.0	48.5	$0.0051 \pm 0.0016 \pm 0.0007$

Table 8: *Medium  $z$ : Cross sections in bins of  $W_{\gamma p}$ ,  $z$  and  $p_{t,\psi}^2$  ( $0.3 < z < 0.9$ ,  $60 < W_{\gamma p} < 240$  GeV).*

$p_{t,\psi}^2$ [GeV <sup>2</sup> ]	$\langle p_{t,\psi}^2 \rangle$	$d^2\sigma_{\gamma p}/dp_{t,\psi}^2 dz$ [nb/GeV <sup>2</sup> ]		
		$0.3 < z < 0.6$	$0.6 < z < 0.75$	$0.75 < z < 0.9$
1.0 – 2.1	1.54	$12.2 \pm 1.2 \pm 1.7$	$14.0 \pm 1.7 \pm 1.9$	$22.6 \pm 2.8 \pm 3.1$
2.1 – 3.5	2.78	$5.93 \pm 0.65 \pm 0.82$	$11.9 \pm 1.33 \pm 1.66$	$11.4 \pm 1.8 \pm 1.6$
3.5 – 5.4	4.38	$3.11 \pm 0.41 \pm 0.43$	$6.14 \pm 0.77 \pm 0.85$	$6.27 \pm 1.03 \pm 0.87$
5.4 – 7.6	6.43	$2.08 \pm 0.26 \pm 0.29$	$2.61 \pm 0.46 \pm 0.36$	$2.72 \pm 0.57 \pm 0.38$
7.6 – 10.0	8.74	$1.17 \pm 0.18 \pm 0.16$	$1.56 \pm 0.27 \pm 0.22$	$2.57 \pm 0.54 \pm 0.36$
10.0 – 13.5	11.6	$0.530 \pm 0.103 \pm 0.074$	$1.14 \pm 0.208 \pm 0.158$	$1.01 \pm 0.24 \pm 0.14$
13.5 – 20.0	16.4	$0.184 \pm 0.039 \pm 0.026$	$0.547 \pm 0.113 \pm 0.076$	$0.276 \pm 0.083 \pm 0.038$
20.0 – 26.5	23.0	$0.145 \pm 0.029 \pm 0.020$	$0.143 \pm 0.040 \pm 0.020$	$0.110 \pm 0.039 \pm 0.015$
26.5 – 40.0	32.3	$0.0323 \pm 0.0097 \pm 0.0045$	$0.0296 \pm 0.0169 \pm 0.0041$	$0.0804 \pm 0.0284 \pm 0.0112$
40.0 – 60.0	48.5	$0.0113 \pm 0.0059 \pm 0.0016$	$0.0059 \pm 0.0029 \pm 0.0008$	$0.0057 \pm 0.0033 \pm 0.0008$

Table 9: *Medium  $z$ : Double differential cross sections in  $z$  and  $p_{t,\psi}^2$  ( $60 < W_{\gamma p} < 240$  GeV).*

$W_{\gamma p}$ [GeV]	$\langle W_{\gamma p} \rangle$	$\sigma_{\gamma p}$ [nb]
120 – 150	133.8	$12.1 \pm 1.5 \pm 2.6$
150 – 180	163.9	$12.8 \pm 2.1 \pm 2.5$
180 – 260	213.7	$15.6 \pm 2.5 \pm 3.1$

$p_{t,\psi}^2$ [GeV <sup>2</sup> ]	$\langle p_{t,\psi}^2 \rangle$	$d\sigma_{\gamma p}/dp_{t,\psi}^2$ [nb/GeV <sup>2</sup> ]
1.0 – 2.1	1.54	$3.56 \pm 0.83 \pm 0.68$
2.1 – 3.5	2.78	$1.85 \pm 0.42 \pm 0.35$
3.5 – 5.4	4.38	$1.24 \pm 0.30 \pm 0.24$
5.4 – 7.6	6.43	$0.875 \pm 0.177 \pm 0.167$
7.6 – 10.0	8.75	$0.489 \pm 0.115 \pm 0.095$
10.0 – 13.5	11.6	$0.267 \pm 0.068 \pm 0.053$
13.5 – 20.0	16.4	$0.117 \pm 0.030 \pm 0.024$
20.0 – 40.0	27.8	$0.0197 \pm 0.0044 \pm 0.0043$

Table 10: *Low  $z$ : Differential cross sections in bins of  $W_{\gamma p}$  and  $p_{t,\psi}^2$  ( $0.05 < z < 0.45$ ,  $120 < W_{\gamma p} < 260$  GeV).*

$z$	$\langle z \rangle$	$d\sigma_{\gamma p}/dz$ [nb]
0.05 – 0.15	0.10	$35.1 \pm 8.3 \pm 8.5$
0.15 – 0.30	0.23	$31.1 \pm 4.1 \pm 6.2$
0.30 – 0.45	0.38	$36.7 \pm 4.0 \pm 7.0$
0.30 – 0.45	0.38	$31.8 \pm 3.6 \pm 4.4$
0.45 – 0.60	0.53	$58.7 \pm 4.3 \pm 8.2$
0.60 – 0.75	0.68	$80.2 \pm 5.3 \pm 11.2$
0.75 – 0.90	0.83	$98.7 \pm 7.5 \pm 13.7$

Table 11: *Total  $z$  range: Differential cross sections in bins of  $z$  ( $120 < W_{\gamma p} < 260$  GeV and  $p_{t,\psi} > 1$  GeV). The points at  $z = 0.375$  are statistically correlated, the first one is obtained from dataset II the second one from dataset III.*